A STUDY OF THE EJECTED-ELECTRON SPECTRUM OF AUTOIONIZING LEVELS IN ATOMIC POTASSIUM EXCITED BY ELECTRON IMPACT

by

GASSEM KAVEI

A thesis submitted for the degree of

Master of Philosophy

Department of Physics
University of Southampton
September 1977

ACKNOWLEDGEMENTS

I should like to express my gratitude to Dr. T.W. Ottley for his many helpful comments and suggestions, providing the answers to many of my problems, and for invaluable discussions. In many ways this work owes a great deal to him.

I am indebted to Dr. K.J. Ross, my supervisor, for giving me the opportunity to study this subject, his many helpful suggestions and for reviewing this thesis.

I should also like to thank V. Pejčev, Dr. M.D. White, H. Bolouri and D. Rassi for their cooperation throughout this research.

Finally my great thanks to my brothers and sisters for their support and encouragement.

CONTENTS

Abstract

Faculty of Science

Physics

Master of Philosophy

A study of the ejected-electron spectrum of autoionizing levels in atomic potassium, excited by electron impact.

GASSEM KAVEI

Ejected-electron spectra of potassium vapour autoionizing levels, excited by electron impact, have been obtained. The experiment was performed with two different spectrometers, denoted Apparatus 1 and Apparatus 2 in the text.

In Apparatus 1, electrons were detected at 90° to the direction of the incident electron beam. The energy resolution of spectra obtained was 55 meV, and incident electron energies of 30, 60 and 400 eV were used. Ejected electrons in the energy range 13.8-21.1 eV were studied.

Apparatus 2 was a high resolution, variable-angle electron spectrometer and spectra were taken at 50° and 75° with respect to the incident electron beam. An energy resolution of 20 meV was achieved. Spectra were recorded in the 3-20.3 eV ejected-electron energy range, using incident electron energies of 30, 40, 60 and 400 eV.

Comparison is made with earlier ejected-electron spectroscopy data of Ottley & Ross (1975), photoabsorption measurements and theoretical calculations. Excellent agreement is obtained with the photoabsorption data of Mansfield (1975a). A total 87 lines have been observed, 38 of these for the first time. These latter lines were detected on the spectra taken at low incident energies and are therefore, expected to be due to optically forbidden transitions. In addition, three lines of the KII spectrum have been detected, and tentatively assigned.

CHAPTER 1

INTRODUCTION

1.1 Spectroscopy

The study of the spectra of atoms and molecules leads to a detailed knowledge of their structures, transition probabilities and energy levels.

Perhaps the most important aspect of atomic spectoscopy is the determination of energy levels. The experimental methods employed to do this consist fundamentally of measurements of either energy or frequency; the energy difference between two levels involved in a transition determines the frequency of the radiation which can be emitted or absorbed. The basic equation for this process is the quantum condition $h\nu = E_1 - E_2$ where h is Planck's constant, ν is the frequency of the radiation and E_1 and E_2 are the initial and final energy states or levels of the system emitting or absorbing that radiation.

The problem for the experimental spectroscopist is thus to measure the frequency or energy of the transition as accurately as possible, this entailing consideration of parameters such as line widths, intensities and standards of frequency. Experimental data for a given system need a good theoretical background for their interpretation, which must be able to predict a comprehensive picture of the energy level system. When this theoretical explanation of the energy level system has been obtained it can be used, in turn, to give information concerning the forces and interactions which exist inside the atom being studied. The different forces and interactions which produce and modify the energy level system vary enormously according to the frequency or energy range being investigated.

Above the ionization limit there exist excited states of the neutral atom, which may decay spontaneously to give the ion and an ejected electron in a process known as autoionization. These

autoionizing states can be studied by a variety of methods (see below), and fall into three main categories:

1. Those immediately above the first ionization potential, such as the $O^+(^2D)nl$ and $O^+(^2P)nl'$ levels which lie in the $O^+ {}^4S$ continuum.

2. Inner shell excitations, such as the (core)$3p^5 4snl$ configuration of potassium.

3. Doubly-excited states, such as the $3p^6 nlnl'$ $n \geq 4$ configuration of calcium.

It should be noted that some atoms have single-electron inner-shell excited states below the first ionization potential. For example $3d^9 4s$ is the first excited state of copper (ground state $3d^{10} 4s$).

Some atoms possess bound doubly excited states with energies which lie below the first ionization potential. The $3p^2\ {}^3P_1$ term of magnesium is an example of this. However, double-electron excited states are almost always "quasi-bound" and have energies in excess of the first ionization threshold. In this case the atom may autoionize ejecting an electron, or decay by photon emission, although the probability for the latter process is usually much less than that for autoionization.

1.2 The Methods of Investigating Autoionization

Autoionizing states in atoms were first observed as diffuse lines in the absorption spectra in the region above the ionization threshold by Fues (1927). Such autoionizing states in atoms are observed as series of highly excited Rydberg states converging on limits which coincide with excited states of the ion. Often the lines exhibit asymmetric profiles.

The methods used for the observation and investigation of autoionization in atoms are:

1. Photon impact. This gives rise to only those resonances which may be excited by an electric dipole transition from the ground state.

2. Photon impact followed by energy analysis of the ejected electrons. This allows for multipole transitions but excludes the possibility of a change of spin.

3. Electron impact: this allows the possibility of studying all possible autoionization states. The low energy electron impact technique is a convenient method for the study of optically forbidden transitions (spin, parity, or both, and J) that are inaccessible by photon absorption. Under such conditions the optical selection rules do not apply. However, at high incident electron energies where the Born approximation is valid, and where the momentum transfer vector is perpendicular to the direction of the incident electron beam, electron excitation is similar to photo-absorption, and optically allowed dipole transitions predominate. Because, at low incident electron energies there is a considerable rotation of the momentum transfer vector, parity invariance (magnetic dipole and electric and magnetic multipole) can be excited. Also at low incident energies electron exchange (spin exchange) mechanisms predominate causing "singlet-triplet" type transitions.

4. Impact by ions with $Z>1$, The collision of fast ions with target atoms allows the incoming ion to be excited to optical or optically-forbidden autoionizing states.

In electron impact, the study of autoionizing states may be made by collecting the scattered electrons (energy-loss spectroscopy) corresponding to excitation of the states, by observing the electrons ejected on decay into the degenerate continuum, or by collecting the ions resulting from the latter decay. High energy resolution is easier to achieve by collecting the ejected electrons than by

collecting the scattered particles. In the former method there is no dependence on the energy resolution of the incident beam, and consequently the beam may be taken directly from an electron gun; this leads to better signals than in the case of the second method.

1.3 Autoionization in Potassium Atoms

Alkali-metal atoms are perhaps more interesting than other metals from a theoretical viewpoint due to their simple single-valence electron structure. Also they are experimentally easy to handle.

In particular, potassium has been the subject of many investigations. The earliest photo-absorption experiment to reveal the autoionizing levels of potassium was carried out by Beutler & Guggenheimer (1933). They obtained the potassium absorption spectrum below 1,000Å and observed the strong doublet $3p^6 4s^2 S_{1/2} \rightarrow 3p^5 4s^2\ ^2P_{1/2,\ 3/2}$ at about 660Å

Hudson & Carter (1965) reported an atomic absorption cross-section measurement of neutral potassium from the principal series limit at 2856Å to 1150Å and made comparison with the theoretical data of Seaton (1951) and Bates (1947). Later Hudson & Carter (1967) continued their atomic absorption cross-section measurement of potassium vapour between 580 and 1,000Å , and in the region between 580 and 685Å found several autoionization lines.

The most recent investigation of autoionization in potassium using the photo-absorption technique has been made by Mansfield (1975a) in the range 700-350Å ; this work revealed at least 140 new features which were attributed to excitation of a 3p electron. Eight additional lines were observed in the region between 120-10Å by Mansfield (1975b), attributable to the excitation of an electron from the 2p inner shell. In these papers, Mansfield used Hartree-Fock calculations to interpret

more than 50 features, mainly at longer wavelengths, and to give tentative assignments.

Atomic structure investigation with photo-absorption techniques is restricted to optical selection rules ($\Delta S=0$ $\Delta L=0, \pm 1$ $L=0 \not\rightarrow L=0$ $\Delta J=0, \pm 1$ $J=0 \not\rightarrow J=0$, and parity change), precluding observation of the important optically-forbidden transitions.

Feldman & Novick (1967) observed discrete atomic energy levels lying between the first and second ionization potentials in the alkali-metals which are metastable against both autoionization and radiative decay. The experimental method was the atomic beam magnetic resonance technique. The metastable atomic beam was produced by electron bombardment of neutral atoms. They reported the excitation energies, cross sections, and natural lifetimes, and gave tentative spectroscopic assignments for metastable autoionizing levels in the alkali-metals, including potassium. Sprott and Novick (1968) obtained improved data for the same experiment. They observed two autoionizing states in potassium.

Metastable autoionizing states of Li and K were reported by Slavik et al (1975) in a mass spectrometer experiment. They used electrons to excite the potassium atoms to the quartet autoionization states $3p^5 4s 3d\,^4F_J$ and deduced a lifetime for these states greater than 10^{-6} sec.

Pegg et al (1975) have investigated the ejected-electron spectrum resulting from the passage of a 70 keV K^+ beam through a He gas target in the ejected-electron energy range 12.5 to 24 eV. A number of optically-forbidden autoionizing states of potassium were observed.

Trajmar & Williams (1976) have studied autoionizing levels in potassium vapour using the technique of high resolution electron energy-loss spectroscopy. With an incident electron beam energy of 100 eV,

several lines were found in the excited state energy range 18.5 to 25 eV. It should be noted that this incident energy was not high enough to allow unqualified application of the Born approximation; optically forbidden transitions are almost certainly present at this energy.

Inner-shell excitation-ionization in potassium by electron impact has been studied by Nygaard (1975). He observed, under poor resolution conditions, an autoionization peak in potassium at 20 eV, which he attributed to excitation of the $3p^5 4s^2\ ^2P_{1/2,\ 3/2}$ levels.

Ottley & Ross (1975) investigated the autoionizing levels of potassium by measuring the ejected electron spectrum at 90° to the direction of an incident electron beam. Spectra were taken at 29 and 500 eV incident electron energies. The data was compared with ultraviolet absorption spectra, and about 25 new features were revealed.

In this thesis the ejected-electron spectrum of potassium vapour is presented, obtained using two different ejected-electron spectrometers. The basic apparatus used for the experimental investigation is a crossed-beam electron spectrometer which observes the ejected-electron spectrum at a fixed angle of 90° to the direction of the incident electron beam; a detailed description of the apparatus is given in Chapter 3.

The resolution in the spectra obtained using this fixed angle apparatus was approximately 55 meV (full width at half maximum - FWHM).

The second spectrometer was constructed to observe ejected-electron spectra at different angles with respect to the incident electron beam. Using this apparatus, for all spectra, the resolution in the ejected electron spectrum FWHM was about 20 meV. This improved resolution resulted in many lines being observed which were not

resolved in the first apparatus. This second apparatus is also described in Chapter 3.

Comparisons have been made between the present results and the theoretical and photo-absorption data of Mansfield (1975a); the agreement is good.

Also, comparisons have been made with the theoretical work on autoionizing states in potassium of Martin et al (1969), who calculated energies for the $3p^5 3d4s$ and $3p^5 4s4p$ configurations.

In addition, in the present work, three lines were observed using a 400 eV incident electron beam, corresponding to the Coster-Kronig transitions $3s3p^6 4s \rightarrow 3s^2 3p^5\ ^2P_{3/2,\ 1/2}$ and tentatively, $3s^2 3p^4 4s^2 \rightarrow 3s^2 3p^5$.

CHAPTER 2

THEORY

2.1 General Aspects

2.11 Transitions and Selection Rules

Radiative electronic dipole transitions represent the interaction between atoms and a radiation field; only the electric field component is considered. A complete theoretical treatment requires the use of quantum electro-dynamics. However, most of the essential results can be obtained by simpler methods in which the electro-magnetic field is introduced as a time dependent purturbation. The perturbation produces a certain probability of finding the electron in a different final state ψ_j from the initial state ψ_i, provided that the frequency of the oscillating field obeys the relation $h\nu = |E_j - E_i|$. By expanding the interaction between the electron and the electro-magnetic field as a power series the transition probability can also be obtained as a series, of which the first term is proportional to the electric dipole strength or transition moment for the two states concerned $|\langle j|\underline{er}|i\rangle|^2$, where $\langle j|\underline{er}|i\rangle = \int \psi_i^* \underline{er} \psi_j d\tau$. Higher terms in the expansion lead to electric quadrupole and magnetic dipole radiation.

The selection rules for atoms in the L-S coupling scheme for electric dipole radiation are, using conventional notation:

$$\Delta S = 0, \quad \Delta L = \pm 1, \quad \Delta J = 0, \pm 1 \text{ but } J = 0 \not\rightarrow J = 0$$

Selection rules hold strictly only for free atoms. External fields due to the ions in a discharge or even to neighbouring neutral atoms can give rise to observable enforced transitions.

In addition, the ΔL and ΔS rules may be broken, particularly in the heavier elements where L-S coupling is no longer a good description.

For example, the singlet-triplet intercombination line $6^1S_0 \rightarrow 6^3P_1$ is the second strongest line in the mercury spectrum, 2537Å and is often called the resonance line (incorrectly).

Transitions forbidden by electric dipole selection rules may occur by magnetic dipole or electric quadrupole radiation, for which processes the selection rules are different. In particular, the parity rule for these transitions is even↔even or odd↔odd. This allows transitions between terms in the same configuration which are forbidden for electric dipole radiation. Their transition probabilities are however smaller by factors of the order of 10^5 and 10^8, respectively in the visible region. The upper levels of such "forbidden" lines are called metastable levels, which autoionize at a slower rate via the weaker magnetic interactions.

2.12 Quantum Defect

In series of the type (Core)nl of neutral atoms, the energy level of the term in the series can be found approximately from the following equation;

$$T_n = \frac{RZ^2}{(n - \sigma_{n,l})^2} \qquad (2.121) \qquad \text{(Kuhn, 1969)}$$

where T_n is the energy of the state measured from the series limit ($n=\infty$); R is the Rydberg constant, n the principal quantum number, and $\sigma_{n,l}$ is the quantum defect, Ze is equal to the charge of the nucleus plus that of the exposed shell of electrons. Z=1, 2, 3,...for neutral, singly ionized, doubly ionized,...atom. This formula is known as the Rydberg-Ritz formula. The quantum defect arises due to electron orbits penetrating the core, resulting in the effective charge seen by those electrons being more than one.

This formula is also useful for the comparison of the corresponding terms in isoelectronic elements, where it describes the variation of T_n as a function of Z fairly well.

The application of equation 2.121 plays an important role in the assignments of lines to series, both in optical spectroscopy, and ejected-electron spectroscopy. The quantum defect is a function of n and l and is described empirically by the equation:

$$\sigma_{n,l} = \alpha(l) - \frac{\beta(l)}{n^2}$$

Thus, to first order, the quantum defect is constant for a given series.

2.13 Coupling Schemes

The L-S (see Russell & Saunders 1925) coupling scheme used in this section is valid only when the magnetic interaction in the atom is much smaller than the electrostatic interaction and the L and S vectors are strongly coupled.

For ground and low excited configurations, the coupling of the angular momentum vectors $l_1, l_2, l_3 \cdots$ and spin vectors $s_1, s_2, s_3 \cdots$ is usually best described for elements of low and medium atomic number by (L-S) coupling

$$\left[(l_1, l_2, l_3 \cdots)L, (s_1, s_2, s_3, \cdots)S\right] J$$

When this is not the case another coupling scheme must be used; (j-j) coupling for example. In this coupling scheme J is the only quantum number that can be defined in addition to the n,l of the individual electrons. The coupling of the $l_1, s_1; l_2, s_2; l_3, s_3; \cdots$ vectors of high atomic number elements is usually described by (j-j) coupling

$$\left[(l_1, s_1)j_1, (l_2, s_2)j_2, (l_3, s_3)j_3...\right] J$$

A further coupling scheme was given by Racah (1942). This coupling is nominated as $j_c K$ coupling. Cowan & Andrew (1965) have considered the coupling in two-electron spectra, when the outermost electron of a heavy element is highly excited, and particularly when it has a high value of l. In such cases the configuration is highly asymmetric in the two electrons, and the symmetric couplings (L-S), (j-j) are usually no longer good approximations. Observed structures frequently show a striking tendency of the levels to occur in pairs. Racah (1942) has shown that the conditions responsible for this pairing are obtained by a type of coupling for two-electron spectra:

$$\left[(l_1 s_1), l_2)K, s_2\right] J$$

The occurrence of pairs of lines is the result of the weak spin-orbit interaction of the outermost electron. The (l_1, l_2) interaction of the highly excited outermost electron with the core (e.g. 5f with $3d^9$ in Cu II) becomes smaller than the (l_1, s_1) spin-orbit interaction of the core electron, at the same time the (l_2, s_2) spin-orbit interaction of the outermost electron is weak compared with (l_1, l_2). Therefore two levels with different J value have nearly the same energy, (see Shortley & Fried, 1938).

2.2 Autoionization

The interactions discussed in Section 2.1 for an atom in zero external field have all been based on the concept of single well-defined configurations. The assumption is that a definite (n, l) value can be allocated to each electron.

A comparison of theoretical and experimental values of energy levels and transition probabilities shows that this assumption is

not always justified. It is often necessary to mix into the basic configuration contributions from one or more other configurations in order to describe the system properly. With no external field perturbation to affect the symmetry, configurations can only interact if they have the same parity, in contrast to the Stark effect. The other rule is that, within two such configurations only terms of the same J can interact with one another. The strength of the interaction, or the amount of mixing, falls off inversely as the energy difference between the terms.

Of particular interest is the configuration mixing between a bound state and an adjacent ionization continuum, which gives rise to autoionization. In a simple atomic model of electron excitation, only the valence electron is excited and all terms converge to the same limit, the ionization potential, corresponding to the ion in its ground state plus the electron with zero kinetic energy. In the continuum states beyond the series limit the electron has finite kinetic energy. But, as mentioned earlier there exist bound states equal in energy to the continuum states due to the excitation of an electron from an inner shell, For example, one of the "p" electrons from the $3p^6$ closed shell in potassium. The interaction between one of these bound states and the adjacent continuum state of the same energy leads to a mixing of the wave functions and hence to a mixing of the properties of the two states. The bound state becomes in some measure a piece of continuum and is thereby broadened. One can also think of the mixing as denoting a certain probability of finding the system in the ionized-state. In other words, of undergoing a radiation less transition, as shown schematically in Figure 2.21. This process is known as autoionization. The process of excitation and autoionization is represented by:

$$A + e(E_1) \rightarrow A^* + e(E_3) \qquad (12)$$

where A* has energy E_2 above the ground state and $e(E_3)$ is the scattered electron of energy E_3

$$A^* \rightarrow A^+ + e(E_j)$$

where $e(E_j)$ is the ejected electron of energy Ej, and

$$E_3 = E_1 - E_2$$

where $E_2 \simeq$ ionization potential + E_j

Autoionization transition probabilities may be as high as $10^{13}sec^{-1}$ in contrast to a typical value of 10^8sec^{-1} for an allowed radiative transition. The natural width of a line depends on the decay life time. Not all excited states above the ionization level can undergo autoionizing transitions.

The selection rules for autoionizing transition have been discussed by Rudd & Smith (1968) covering only (L-S) coupling. For (L-S) coupling the parity and L value rules can be combined to yield the following selection rules:

1. If neither state (excited state and continuum) is an "S" state, the autoionizing transition is not forbidden

2. If one of the states is an "S" state then,

   a) If the parities of the configurations are the same then the other state must be a S, D, G...state.

   b) If the parity is different then, the other state must be a P, F, H...state.

Since an autoionizing electron is ejected carring spin of $\frac{1}{2}$, the spin rule can be restated as follows:

The multiplicities (2S+1) of the initial excited state and of the final ion state must differ by unity.

Because of the possibility of electron exchange between target and projectile in particle excitation, the following rules hold for the excitation of neutral states:

Autoionization process

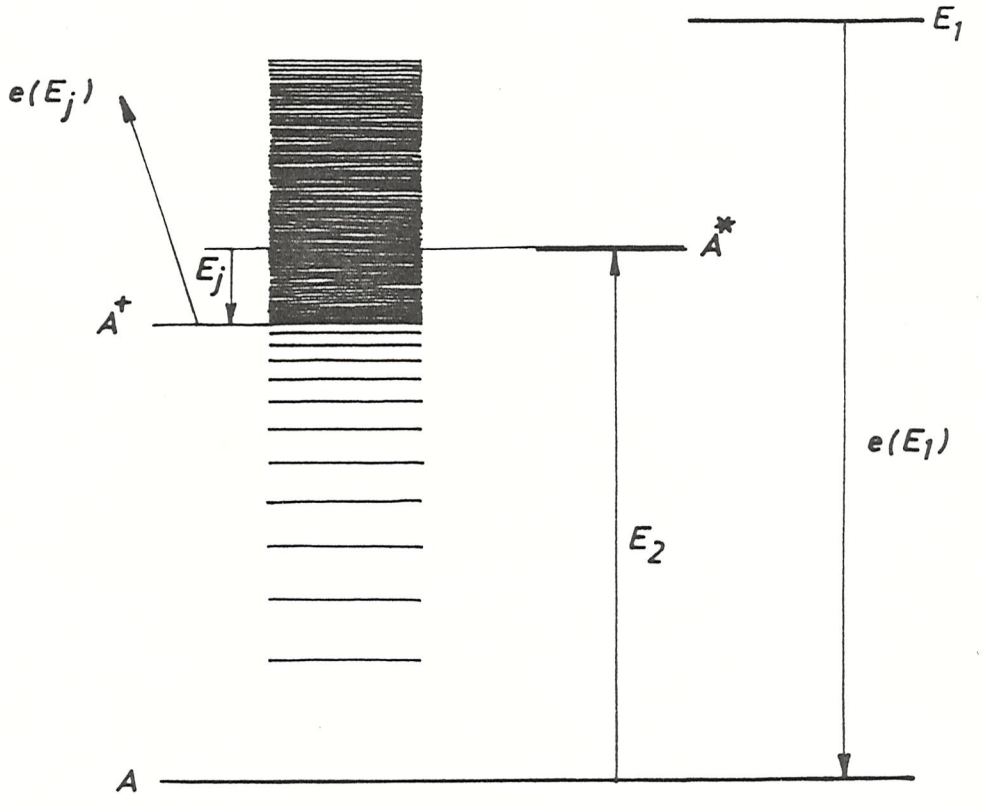

1. For atoms subjected to L-S coupling the multiplicity can change at most by a number equal to twice the number of electrons in the projectile.

2. For atoms not subjected to L-S coupling, or for atoms formed for the dissociation of molecules, there is no restriction of the change of spin, except that the total spin must be conserved.

2.21 Autoionization Theory

The perturbation theory for a case involving degenerate eigen functions is employed to describe the autoionization process, a simple case of autoionization (one discrete state interacting with a continuum in hydrogen) may be used to consider this theory. Massey & Burhop (1969) have calculated the scattering of s-wave electrons by hydrogen, ignoring exchange effects, where the total Hamiltonian is:

$$H\Psi=(H_0+H_1)\Psi=E\Psi \qquad 2.211$$

where
$$H_0=-\left(\frac{h^2}{2m}\right)(\nabla_1^2+\nabla_2^2)-e^2(1/r_1+1/r_2) \qquad 2.212$$

and
$$H_1=e^2/r_{12} \qquad 2.213$$

r_1, r_2 represent the coordinates for the atomic electron and scattered electron respectively relative to the proton. The interaction H_1 represents a small perturbation which vanishes as the separation between the projectile and atom increases.

The wave function for the doubly-excited state $\phi(\underline{r_1}, \underline{r_2})$ can be expressed in terms of products of eignfunctions of two excited states χ_a, χ_b of energies ϵ_a and ϵ_b respectively.

$$\phi(\underline{r_1}, \underline{r_2})=\chi_a(\underline{r_1})\chi_b(\underline{r_2}) \qquad 2.214$$

$$H_0\phi=(\epsilon_a+\epsilon_b)\phi \qquad 2.215$$

where $\epsilon_a+\epsilon_b=E_d$ in zero order approximation. In first order

approximation, the energy of the configuration will be

$$E_d = \epsilon_a + \epsilon_b + \langle \phi | H_1 | \phi \rangle \qquad 2.216$$

$$E_d = \langle \phi | H | \phi \rangle \qquad 2.217$$

The continuum eigenfunction with energy E

$$\psi_E(\underline{r}_1, \underline{r}_2) = \chi_0(r_2) F_0(E - \epsilon_0, \underline{r}_1) \qquad 2.218$$

χ_0 is the wave function for the ground state of the atom with energy ϵ_0 and is orthogonal to χ_a, and $F_0(\underline{r})$ is the wave function of an electron in the potential field of a hydrogen atom with energy $E-\epsilon_0$. F_0 may be chosen as real and form an orthonormal set.

$$\langle \psi_{E''} | H | \psi_{E'} \rangle = E' \delta (E'' - E') \qquad 2.219$$

$$\langle \psi_E | H | \phi \rangle = \langle \psi_E | H_0 | \phi \rangle + \langle \psi_E | H_1 | \phi \rangle ,$$

$$= (\epsilon_a + \epsilon_b) \langle \psi_E | \phi \rangle + \langle \psi_E | H_1 | \phi \rangle$$

$$= \langle \psi_E | H_1 | \phi \rangle \qquad 2.2110$$

Because ψ_E and ϕ are orthogonal, $\langle \psi | \phi \rangle = 0$

finally $$\langle \psi_E | H | \phi \rangle = V_{E\phi} \qquad 2.2111$$

where, if the interaction term H_1 is infinitely small $V_{E\phi}$ vanishes, and, because the functions ψ_E are normalized per unit energy range, $V^2_{E\phi}$ has the demensions of energy.

The three equations 2.217, 2.219, 2.2110 are similar to those used to discuss perturbation theory applied to a discrete degenerate state, (Massey & Burhop, 1969). The analysis applies to any system for which these three relations exist.

The interaction of the continuum configuration and discrete states generates an additional phase shift, $E(\sigma)$. This is very small if the continuum energy differs greatly from discrete-level energy, but changes

rapidly by π in going through an energy range of order $(V_{E\phi})^2 = \frac{\Gamma}{2\pi}$ about the resonance value $E_r = E_d + \Delta E$. In other words there is an elastic scattering resonance of width $(V_{E\phi})^2$.

2.3 Fano Profile

Autoionizing lines, in addition to being very broad, can be asymmetric. The exact form of the profiles was first calculated by Fano (1961). An example of asymmetric absorption lines are shown in Figure 2.31. The absorption at some distance from the line is the ordinary continuous absorption from the ground state to the continuum above the normal series limit. The autoionizing transition forms a resonance in the continuum of changing phase in some cases, and may rise steeply on one side to a peak value and drop on the other to zero before going back to the unperturbed continuum level.

The interaction cross section is given by Fano & Cooper (1965);

$$\sigma(E) = \sigma_A \left[\frac{(q+\epsilon)^2}{1+\epsilon^2} \right] + \sigma_B \qquad 2.31$$

where σ_A is the resonant cross-section for that part of the continuum which interacts with the autoionization level and σ_B is the non resonant cross-section for that part which does not. q is a shape profile parameter or profile index related to the strength of the interaction between the line and the background continuum; E is energy of the state, and ϵ is a reduced-energy variable given by $\epsilon = \frac{E-E_r}{\frac{1}{2}\Gamma}$ where E is the electron energy, E_r is an idealized resonance energy depending on a discrete autoionizing level of the atom, and Γ is the line width. The factor $\frac{(q+\epsilon)^2}{1+\epsilon^2}$ gives the shape of the resonance.

When q is large and σ_B is small compared to $\sigma_A q^2$, Equation 2.31 reduces to a Lorentzian profile of the form:

$$\sigma(E) = \sigma_A \frac{q^2}{1+\epsilon^2} = \frac{\sigma_{man}}{1+\epsilon^2}$$

where σ_{man} is the cross section at the peak of the line.

Fano line profiles

2.31

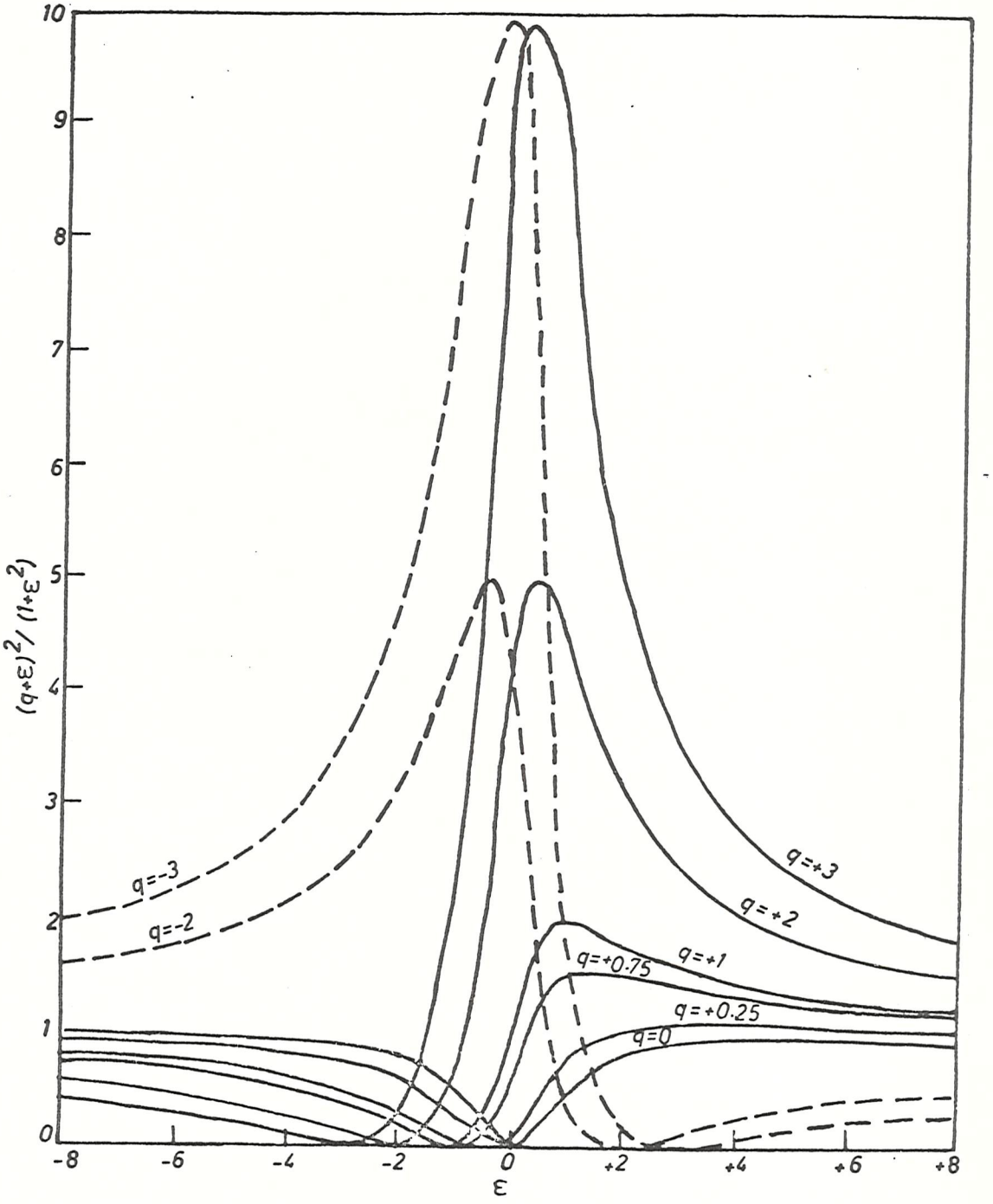

Figure 2.31 is a plot of $\frac{(q+\epsilon)^2}{1+\epsilon^2}$ against ϵ for different q. Where q=0 the autoionizing level appears only as a window in the continuum; a change of sign of q has the effect of producing a mirror image of the profile.

2.4 Auger, Coster-Kronig and Super Coster-Kronig transitions

Excited states caused by inner shell vacancies in atoms may also decay by the emission of electrons or photons. Decay by photon emission leads to the production of characteristic X-rays. The decay of excited states corresponding to inner shell vacancies by electron emission is an autoionization process. In such decay, however, various process have acquired specific names.

The term Auger effect is used to describe both the entire area of inner-shell vacancy decay by electron emission, and those transitions in which a vacancy in an atomic inner-shell leads to vacancies in one or two different principal shells. For example in calcium with configuration $(core)3s^2 3p^6 4s^2$

$$(core)3s^2 3p^6 4s^2 + e(E_1) \rightarrow (core)3s3p^6 4s^2 + e(E_2) + e(E_3)$$

$$(core)3s3p^6 4s^2 \rightarrow (core)3s^2 3p^6 + e(E_4)$$

and in potassium

$$(core)3s^2 3p^6 4s + e(E_1) \rightarrow (core)3s3p^6 4s + e(E_2) + e(E_3)$$

$$(core)3s\,3p^6 4s \rightarrow (core)3s^2 3p^5 + e(E_4)$$

where e(E) is an electron of energy E.

This Auger transition in calcium is given the notation $M_{2,3}\,N_1\,N_1$ and in potassium is given the notation $M_{2,3}\,M_{2,3}\,N_1$.

In the Coster-Kronig-type of transitions (Coster & Kronig, 1935) one of the two vacancies produced in the radiationless decay is in a different sub-shell of the same principal shell that contained the initial vacancy, for example in calcium

$(core)3s^2 3p^6 4s^2 + e(E_1) \rightarrow (Core)3s3p^6 4s^2 + e(E_2) + e(E_3)$

$(core)3s3p^6 4s^2 \rightarrow (core)3s^2 3p^5 4s + e(E_4)$

This Coster-Kronig transition is given the notation $(M_1 M_{2,3} N_1)$.

In Super Coster-Kronig transitions (McGuire, 1972) an initial vacancy can lead to two vacancies in subshells of the same principal shell. For example, in calcium:

$(core)3s^2 3p^6 4s^2 + e(E_1) \rightarrow (core)3s3p^6 4s^2 + e(E_2) + e(E_3)$

$(core)3s3p^6 4s^2 \rightarrow (core)3s^2 3p^4 4s^2 + e(E_4)$

This Super Coster Kronig transition is given the notation $M_1 M_{2,3} M_{2,3}$.

Hence, from an initial 3s inner-shell hole we can have transitions leading to $4s^2$ holes, 3p4s holes or $3p^2$ holes. These are Auger, Coster-Kronig, Super Coster-Kronig transitions respectively, the transitions are listed in order of decreasing ejected electron energy, $e(E_4)$. This ordering is almost exactly true for most of atoms with $Z<58$, (McGuire, 1972).

CHAPTER 3

EXPERIMENTAL

Introduction

Two different sets of apparatus have been used for the measurements described in this thesis. These will be denoted Apparatus 1, and Apparatus 2. Most of the research was carried out on Apparatus 1.

3.1 Apparatus 1

Apparatus 1 is shown schematically in Figures 3.11 and 3.12. The main parts of the apparatus are:

Vacuum pumping system, vacuum chamber, analyser, oven, electron gun, Faraday cup, Helmholtz coils, and electron detector. Further details of each of these parts are given in this chapter.

3.2 Vacuum System

The vacuum pumping system in the experiment consisted of a two-stage rotary pump, backing two oil vapour diffusion pumps (Edwards E04 and Edwards E02). The diffusion pumps (which contained Santovac 5 oil) were each trapped by two chevron baffles. The baffle immediately above the diffusion pump was water cooled, and the second was cooled to approximately -40°C by a refrigerator unit. The vacuum system could be isolated from the diffusion pumps by means of butterfly valves. A magnetic valve (Edwards SVA25) was situated just above the rotary pump to isolate the vacuum system from the rotary pump, and also to let air into the pump in the event of a power failure. Pressure was measured by means of an ionization gauge head, type IG5G, and a Pirani gauge head Model M6A; both gauges were controlled by a combined ionization and Pirani gauge controller (Vacuum Generators IGP3). Further discussion of the details

Schematic diagram of Apparatus 1 *through electron beam*

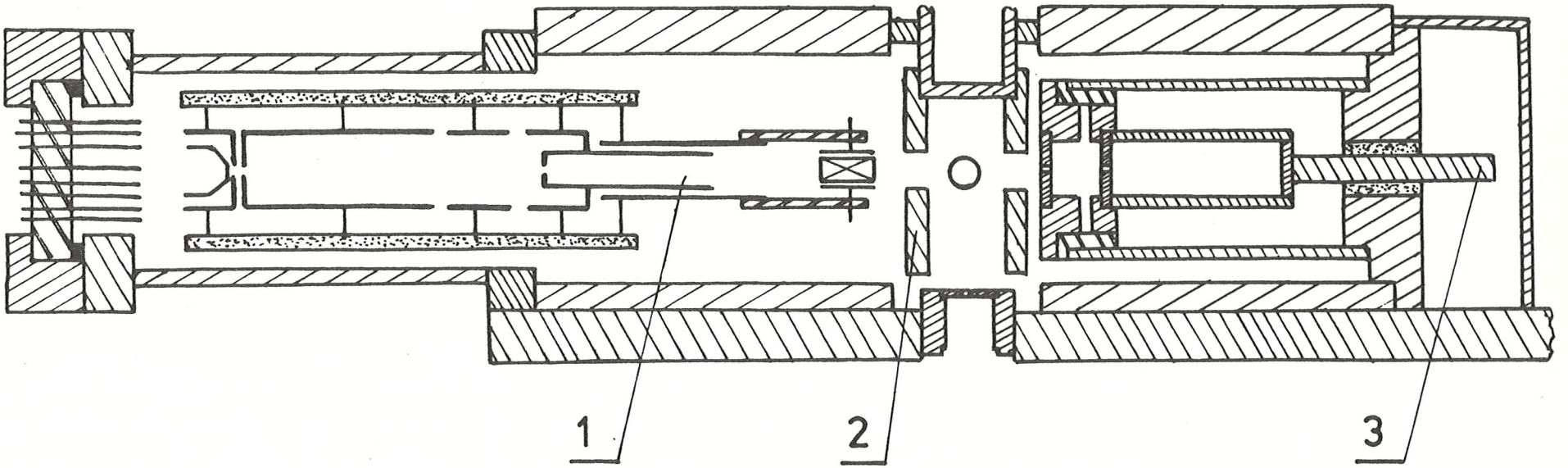

1 - Electron gun

2 - Interaction chamber

3 - Faraday cup

Schematic section of Apparatus 1

through atomic beam

3.12

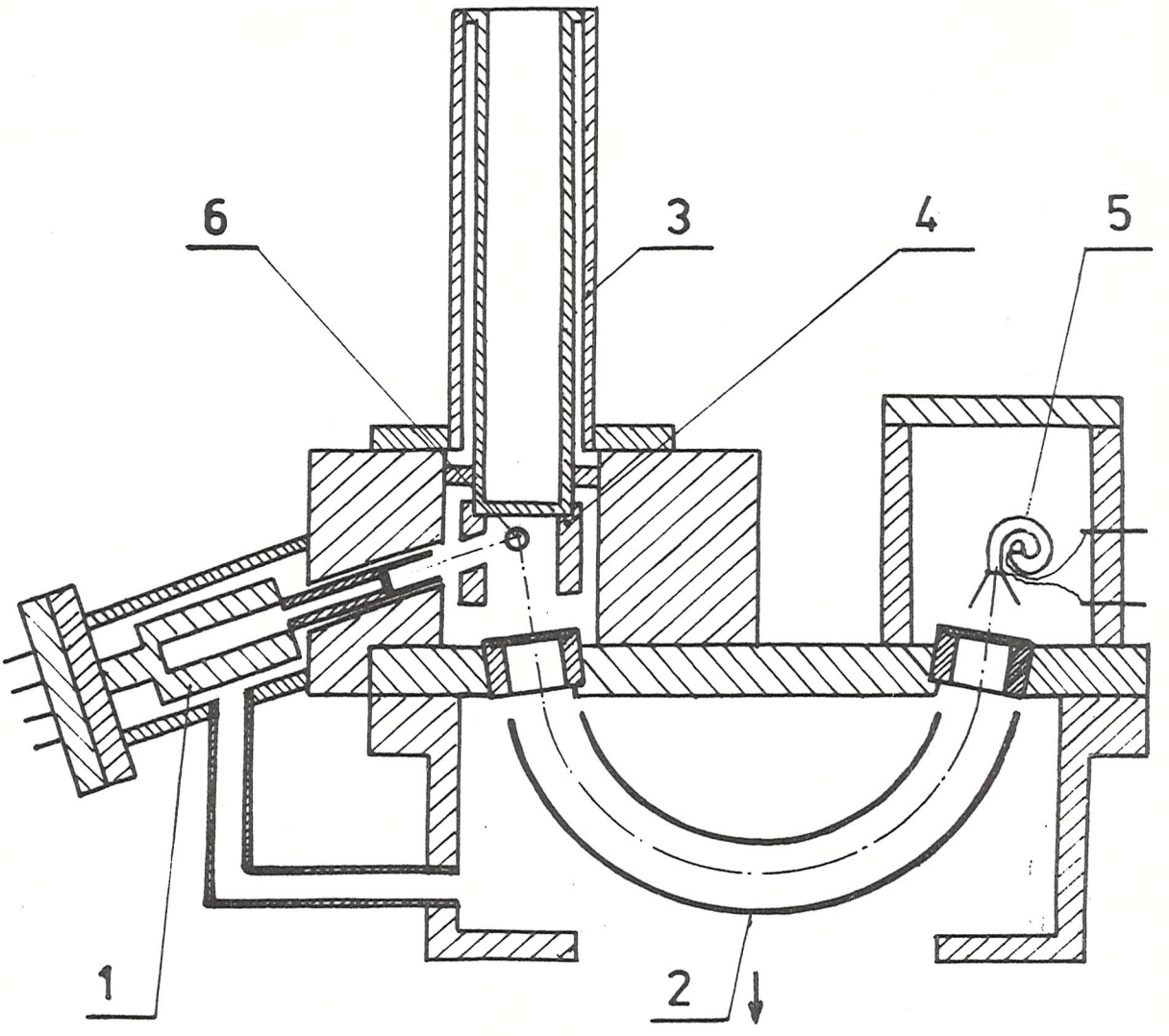

1- *Oven*

2- *Analyzer*

3- *Liquid nitrogen trap*

4- *Interaction chamber*

5- *Channel electron multiplier*

6- *Incident electron beam*

of the operation of the pumping equipment may be found in vacuum system design books, such as Green (1968).

Leak-detecting was performed by spraying methanol on the suspected place and noting whether the reading on the ionization gauge changed. The working pressure was of the order 10^{-6} Torr in the electron gun and analyzer region.

3.3 The Spherical Sector Electrostatic Analyzer

3.31 Theoretical

For analyzing low energy electrons electrostatic analyzers are normally used. The possibility of using a portion of a spherical condenser as an analyzer was first suggested by Aston (1919). The focussing and deflecting properties of the spherical condenser have been described by Purcell (1938). Purcell demonstrated that a group of charged particles homogeneous in energy travel in trajectories with constant major axis in a given field, obeying Kepler's first law, as shown in Figure 3.311. α is the angular separation of the trajectories. When α becomes infinitely small Y_2' vanishes; a slightly diverging bundle of trajectories through P will be nearly focussed at point Q in the exit plane.

Applying a voltage between the electrodes of such an analyzer produces the electrostatic field. Incident particles (electrons) enter the electrostatic field between the spherical surfaces of radii R_1 and R_2 which differ in potential by $V_1-V_2=V$. An electrostatic field at a radius r, which is produced by a difference of potential between two such concentric hemispherical surfaces of radii R_1 and R_2 $(R_2>R_1)$ is given by $\underline{E}=\frac{k}{r^2}$ where k is a constant.

$E=-\frac{dV}{dr}$ where V is the electrostatic potential.

Thus $V = \frac{k}{r} + c$ (1)

Applying the boundary conditions:

$V_1 = \frac{k}{R_1} + c$, and $V_2 = \frac{k}{R_2} + c$ (2)

Therefore, $V_1 - V_2 = k\left(\frac{1}{R_1} - \frac{1}{R_2}\right)$

Therefore, $k = \frac{V_1 - V_2}{\frac{1}{R_1} - \frac{1}{R_2}}$ (3)

And so, $c = \frac{-(V_1 - V_2)}{R_1\left(\frac{1}{R_1} - \frac{1}{R_2}\right)} + V_1$

The electric force F on an electron in an electrostatic field is

$F = eE$ (5)

And the centrigugal force on a particle when it moves in a circular orbit is:

$F = \frac{mv^2}{r}$ (6)

where v is the velocity of the particle, m is the mass, and r is the orbit radius. The electrostatic force, (Equation 5) is equal to the centrigugal force (Equation 6).

Therefore, $eE = \frac{mv^2}{r}$

and $v^2 = \frac{e}{m} \cdot \frac{k}{r}$ (7)

The kinetic energy is:

$E' = \frac{1}{2}mV^2$ (8)

From equations (7) and (8)

$E' = \frac{ek}{2r}$ (9)

From equations (3) and (9)

$E' = eV \frac{R_1 R_2}{R_2^2 - R_1^2}$

If energy of an electron is eV_o electron volts.

$eV_o = eV \frac{R_1 R_2}{R_2^2 - R_1^2}$, and

$$V = V_o\left(\frac{R_2}{R_1} - \frac{R_1}{R_2}\right)$$

From Equation (1) the potential of the inner hemisphere is:

$$V_1 = 2V_o\left(\frac{R_2}{R_1} - \frac{R_o}{R_2}\right)$$

and the potential of the outer hemisphere is

$$V_2 = V_o\left(\frac{R_2}{R_1} - 1\right)$$

Purcell (1938) describes the resolution for the spherical sector analyzer $\Phi = 180^\circ$ shown in Figure 3.311. Suppose the analyzer is set to transmit electrons of energy E_o. An electron with this kinetic energy will travel from the source P, along PT, to the image position Q, passing along the centre-line of the analyzer. If another electron with energy $E_o + \Delta E$, also travels along PT, normal use to the sector entrance plane, it reaches the image plane at point 2, a distance Y_2 from Q. Y_2 is given by

$$Y_2 = \beta R\left(1 + \frac{q}{p}\right) \qquad (10)$$

where $$\beta = \frac{\Delta E}{E_o}$$

Therefore $$\frac{\Delta E}{E_o} = \frac{Y_2}{R\left(1 + \frac{q}{p}\right)}$$

If a slit of width w is placed in the exit plane, it will restrict the energies of transmitted rays, and the instrumental resolution will be

$$\frac{\Delta E}{Eo} = \frac{w}{R\left(1 + \frac{q}{p}\right)}$$

If now an electron of energy E_o passes through the object point P at an angle α to the normal ray it will miss the focus by a small amount Y_2', proportional to α^2.

$$Y_2' = \alpha^2 R\left(\frac{p^2}{q^2} + \frac{q}{p}\right)$$

The effect of this off-axis ray is identical to that produced by an

electron entering the analyzer sector field along the path PT but with an energy $E_o + \Delta E'$. Since Y_2' is known, $\Delta E'$ can be computed from Equation (10):

$$Y_2' = \beta' R\left(1 + \frac{q}{p}\right)$$

where $\beta' = \dfrac{\Delta E'}{E_o}$,

Therefore $$\frac{\Delta E'}{E_o} = \frac{Y_2'}{R\left(1 + \frac{q}{p}\right)}$$

or $$\frac{\Delta E'}{E_o} = \frac{-\alpha^2 R\left(\frac{p^2}{q^2} + \frac{q}{p}\right)}{R\left(1 + \frac{q}{p}\right)}$$

The slit w serves to separate rays of different energies, and, due to the imperfect focussing, electrons at different angle α to the normal ray.

Therefore, $$\frac{\Delta E}{E_o} + \frac{\Delta E'}{E_o} = \frac{w}{R\left(1 + \frac{q}{p}\right)}$$

and thus, $$\frac{\Delta E}{E_o} = \frac{w}{R\left(1 + \frac{q}{p}\right)} + \frac{\alpha^2\left(\frac{p^2}{q^2} + \frac{q}{p}\right)}{\left(1 + \frac{q}{p}\right)}$$

$$\frac{\Delta E}{E_o} = \frac{w}{R\left(1 + \frac{q}{p}\right)} + \alpha^2\left(1 - \frac{p}{q} + \frac{q^2}{p^2}\right)$$

The minimum value of the second term is attained for $q = 2p$. If $p = q$, $\eta = \gamma$ the resolution is given by:

$$\frac{\Delta E}{E_o} = \frac{w}{2R} + \alpha^2$$

which is true for all sector angles Φ .

3.32 Description

In Apparatus 1 the ejected electron spectrum was analyzed using

Spherical sector analyzer

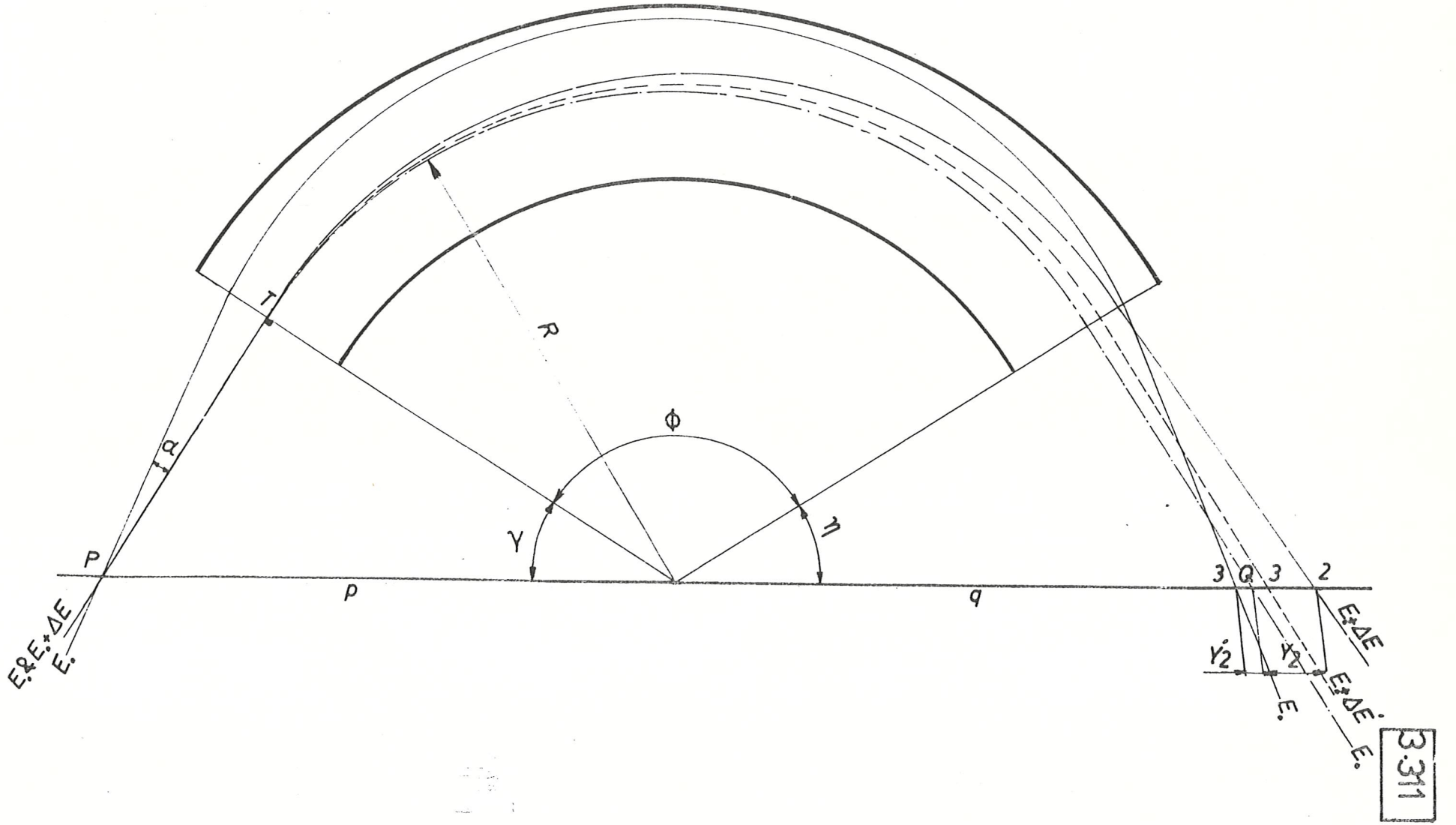

3.311

symmetric 150° spherical sector analyzer with object and image plane at 180°. The mean radius R_o was 10.16cm with R_1 = 9.207cm and R_2 = 11.113cm. The hemispherical sectors were made from non-magnetic stainless-steel, and were sprayed with colloidal graphite solution (Dag). The solution was made up as one part of Dag to three parts of methanol. Dag has a poor reflection coefficient for electrons and was used to reduce reflection and secondary electron emission from surfaces. Also it was used because of its uniform contact potential difference characteristic, which is superior to that of gold. Gold was used by Wickes (1975). The analyzer was insulated from earth and was fixed to the underside of the top flange of the chamber as shown in Figure 3.321. At the entrance and exit of the analyzer were two pairs of slits, denoted Earthed slit 1 and entrance slit, and Earthed slit 2 and exit slit respectively. These slits restricted the angular distribution of the ejected electrons entering the analyzer, and provided a means of retarding or accelerating the electrons. To reduce edge effects, two Herzog diaphragms (Herzog, 1935) were mounted below the entrance and exit slits, which are denoted Diaphragm 1 and Diaphragm 2, as illustrated in Figure 3.321. The slit width of the Earthed slit 1 and Earthed slit 2, the entrance and exit slits and Diaphragm 1 were 0.5mm, and the width of Diaphragm 2 was 4.5mm. The Earthed slits were placed 2.5mm above the entrance and exit slits. 0.05mm thick stainless steel grids were spot-welded on top of the entrance slit and below the Earthed slit 1, as shown in Figure 3.321, to prevent field penetration through the slits, and to enable a uniform retarding or accelerating potentials to be applied between these plates. The slit assembly was made from copper with the exception of the entrance slit and Earthed slit 1, which were made from titanium to facilitate welding of the grids. Titanium is a good non-magnetic metal for use in electron optical systems. A coil of 15 turns of wire was mounted on the analyzer, as shown in Figure 3.321, to cancel residual magnetic fields.

Analyzer

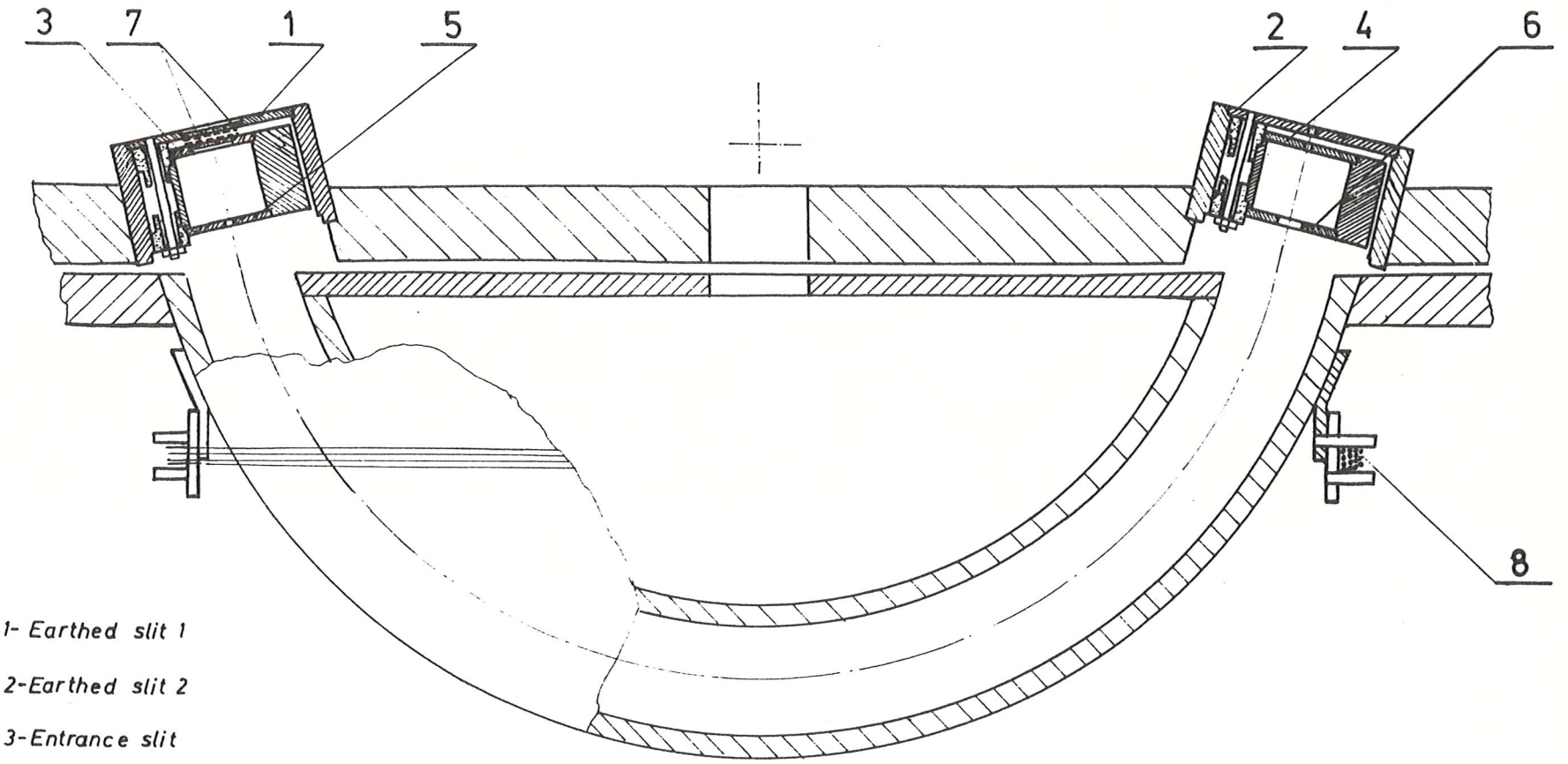

1- Earthed slit 1

2-Earthed slit 2

3-Entrance slit

4- Exit slit

5-Diaphragm 1

6- Diaphragm 2

7- Grids

8- Magnetic field trim coils

3.321

Analyzer circuit

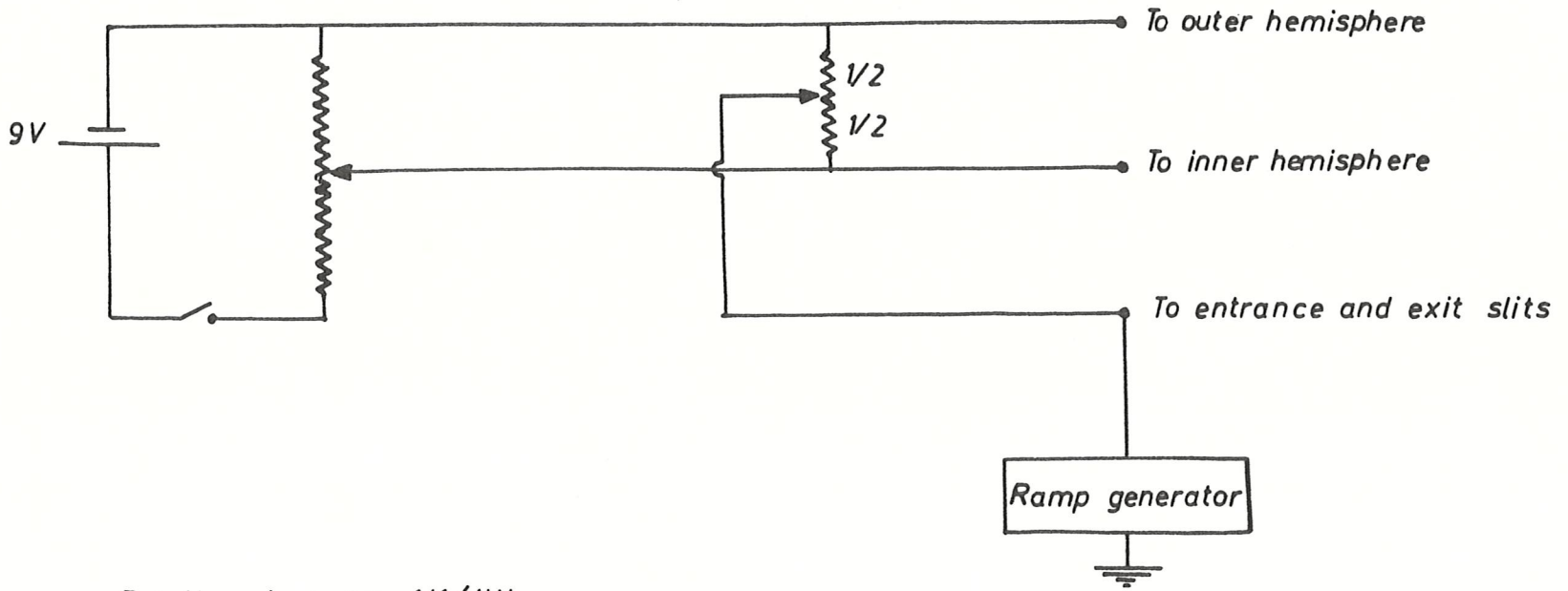

Potetiometers are 1K/4W

In analyzing ejected-electron spectra, an accelerating or retarding voltage ramp was applied to the entrance and exit slits. The analyzer voltage was kept constant; in this way constant resolution spectra were obtained. In the equation $\Delta E_{\frac{1}{2}} = (\frac{w}{2R_o} + \alpha^2)E_o$, where E_o is the analyzer energy, all parameters on the right hand of the equation are constant. The ejected electrons spectrum was analyzed by applying a ramp voltage to both the centre potential of the analyzer and the entrance and exit slits using the circuit shown in Figure 3.322.

3.4 Electron Gun

Many electron impact excitation experiments require electron beams whose energies may be varied from a few eV to some keV. The electron gun can be designed to be capable of forming a beam in which the current is limited only by space charge. Some calculations of electron gun design have been given by Simpson & Kuyatt (1963), but the fields and electron trajectories in the vicinity of the cathode, which have been investigated by Soa (1959), are extremely complex. This makes the design of an electron gun at least partly empirical.

A commercially-made electron gun has been used in the present experiment (Vacuum Generators LEG21). This electron gun is capable of producing a highly collimated beam at energies up to 5 keV and is illustrated in Figure 3.11.

The electron gun was operated by means of the circuit shown in Figure 3.41. Typical voltage parameters necessary for operating the electron gun at energies from 30 to 400 eV are given in Table 3.41. Spectra were obtained for incident-electron energies between 30 to 400 eV. Due to a power supply limitation (500V) it was only possible to operate the gun up to a maximum beam energy of 400 eV. A set of deflectors were added to the LEG21, as shown in Figure 3.11, to compensate for any misalignment

Electron gun circuit

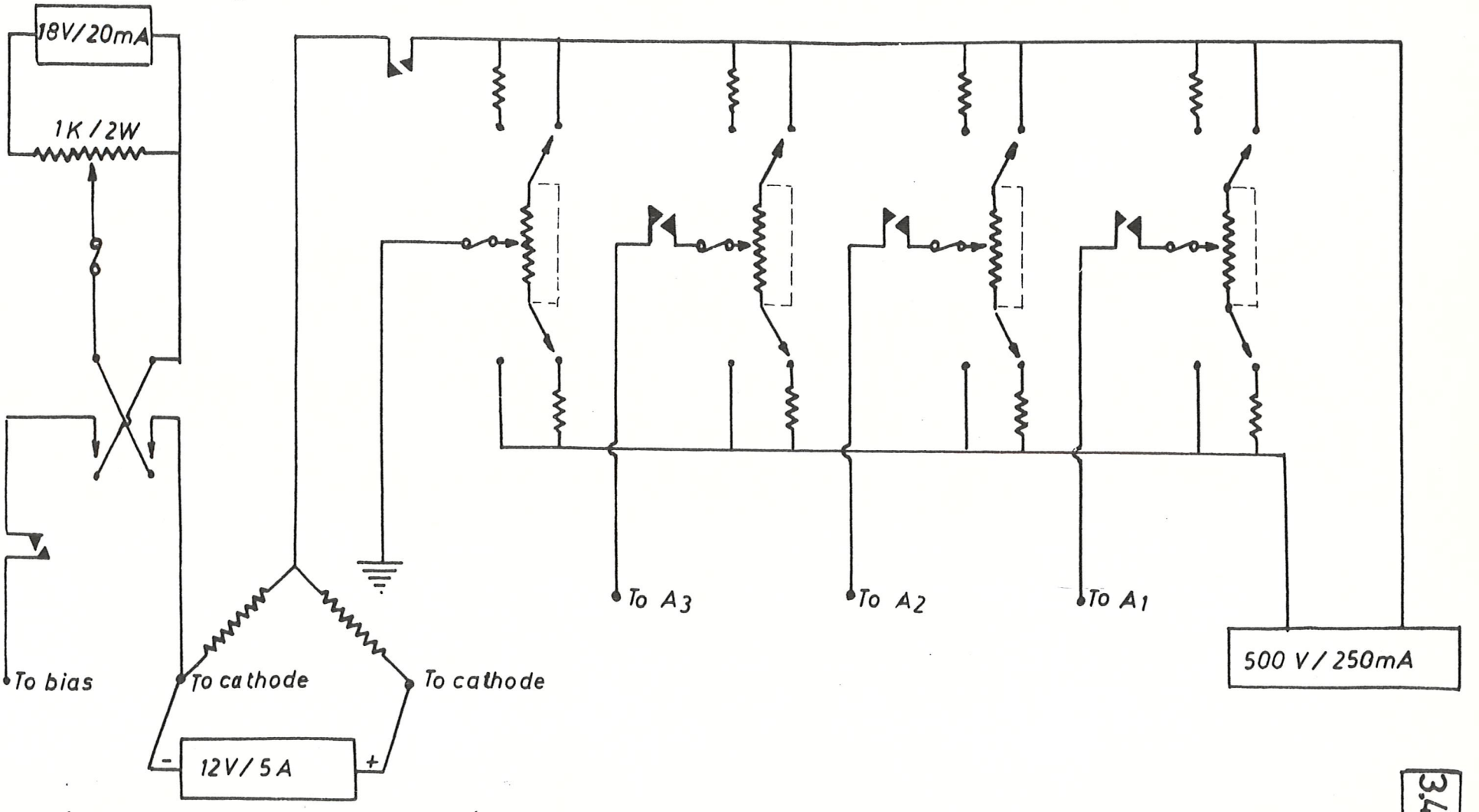

Potentiometers are 30K/4W
Fixed resistors are 33K/2W

3.41

TABLE 3.41

Optimum values of voltages applied to the electron gun for producing a well focussed electron beam at different energies

Type of filament	Filament current Amp	Filament voltage V	Emission mA	Cathode voltage V Incident beam energy -eV	A1 V	A2 V	A3 V	Bias V	Vert. defl. V	Hor. delf. V	Current on the Faraday cup collector μA	Current on front of the Faraday cup μA
Laboratory made	3.1	3.1	+	-390	110	83	380	0.2	28	26	5	+
Laboratory made	3.15	3.3	+	- 30	280	17	180	2.8	29	27	0.012	0.25
Laboratory made	3.15	3.2	0.6	- 30	170	15	210	1.6	30	26	0.04	0.5
Thoriated cathode	2.65	7	1.2	-400	330	18	92.5	5.3	0	12	15	0.75
Thoriated cathode	2.7	7.5	+	- 30	400	8	70	6	6	14	0.5	10

+ not measured

The voltages of A1, A2, A3, Bias, Vertical deflectors and Horizontal deflectors were measured with respect to cathode.

The Cathode voltage was measured with respect to earth

Defelector circuit

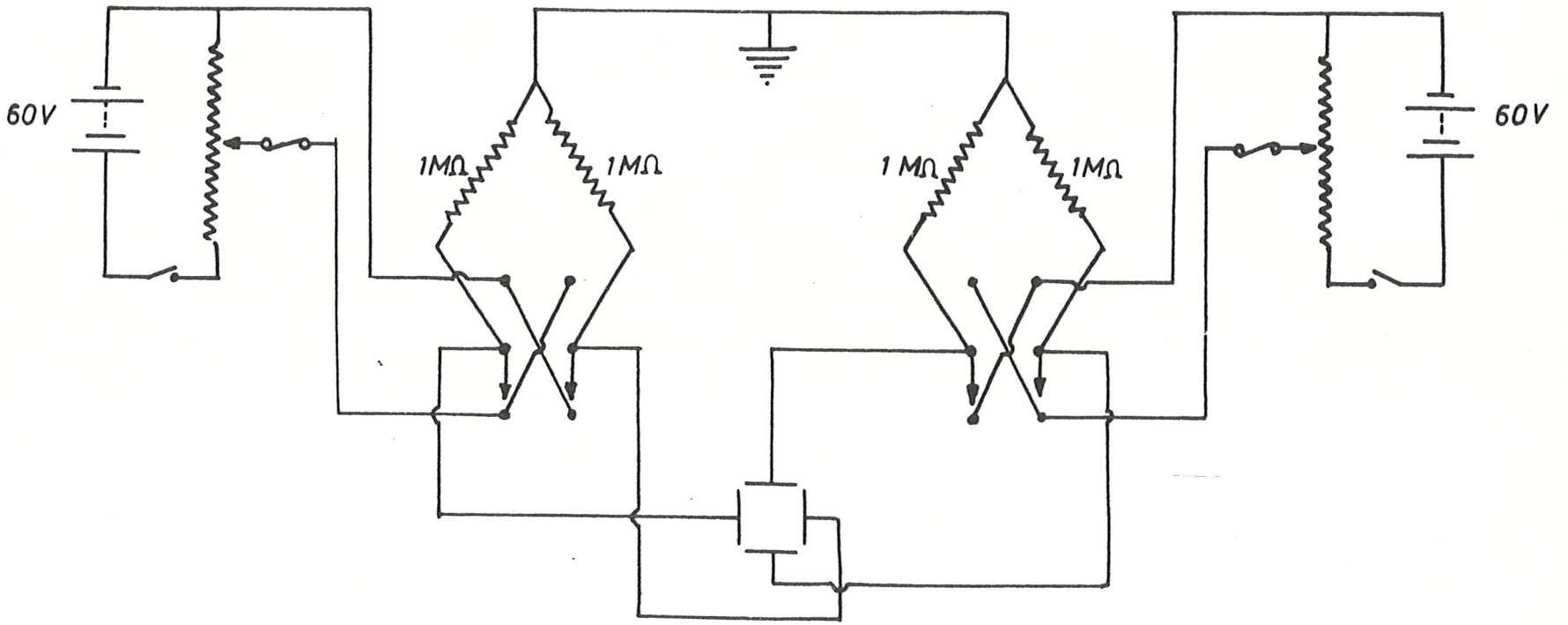

Potentiometers are 30K 4W

3.42

of the beam axis, and stray magnetic fields. The operating circuit for the deflectors is shown in Figure 3.42.

3.41 Cathode

A directly-heated cathode is used in the LEG21. The beam current was found to be very sensitive to the position of the cathode with respect to the bias aperture; 0.2mm was the optimum spacing although small variations in this parameter could be compensated by applying different voltages to the bias.

In this investigation, two types of cathode were used. Initially a thoriated cathode made by Vacuum Generators was used. Spectra at 30 and 60 eV were taken using this cathode. Later a tungsten strip (width 0.7mm thickness 0.04mm) was spot-welded to the cathode base. Because the strip was too thick, the emission of electrons from the surface required a high current. Therefore, after welding, the tip of the strip was etched in a solution of 5g KOH in 200^{cc} water using 3mA at 5V d.c.

The appearance of the laboratory-made cathode was similar to that of the commercially-made cathode. Spectra were taken at 400 eV using this cathode.

An attempt was made to thoriate the etched tungsten strip by electrolysis in a suspension of 3g of thoria (Th_2O_3) in a solution of 1g. of thoriumnitrate in 100ml. of Ethyl alcohol (95%). 67.5V d.c. was applied between the filament and a tungsten anode for about 10 minutes. In this way some thoria was deposited on the filament, but following deposition the filament should have been baked; this was not done. The result was that when it was dried in air the deposit cracked, and when finally the filament was operated in the electron gun the deposit fell

off. As a result, pure tungsten strip was used for the cathode.

Thoriated tungsten wire (0.008" diameter) was also used for making the cathode, but it was difficult to weld, and the emission was low (the beam current as measured in a Faraday cup was about 2μA at 400 eV incident electron energy).

The final beam current achieved was found to be sensitive to the base pressure in the region of the gun. In the present experiment this pressure was normally of the order 10^{-6} Torr. The highest operating pressure possible was 10^{-5} Torr.

3.5 Faraday Cup

In electron impact experiments it is necessary to measure the electron beam current and to have some knowledge of the geometry of the beam. The Faraday cup designed for this purpose is shown in Figure 3.11. The central collector was placed inside an outer screen. On the outer screen an aperture was placed to measure the current to the front of the Faraday cup. The ratio of the current measured on the front plate to that measured in the central collector gives a rough idea of the divergence of the electron beam.

The design of the Faraday cup is important because of the secondary electrons formed when the incident beam hits the central collector. These must be prevented from escaping, otherwise an erroneously small signal, possibly positive, is measured. Lawrence (1926) has stated that the collector should be at least ten times as deep as the diameter of the entrance aperture. The collection efficiency can be further improved by applying a positive potential to the inner collector.

3.6 Oven

The oven was similar to that described by Hertel & Ross (1968),

with some modifications as shown in Figure 3.61. The modifications were designed to minimise the magnetic field associated with the heating elements. To collimate the vapour beam, in addition to the collimated hole structure, an aperture made from copper foil was placed at the top of the oven shown in Figure 3.61.

The oven was made from stainless steel and fitted with upper and lower heating elements as shown in Figure 3.61, so that a temperature difference of 100°C could be maintained between the aperture and the lower part of the oven. The heating elements, which were placed in holes drilled in the oven wall, consisted of heating wire (Kanthal, 0.5mm diameter) fitted in twin-bore ceramic tubes. Two power supplies (3A, 30V d.c.) were used for the heaters. Since the d.c. heating currents flow in opposite directions in the ceramic tube the net magnetic field is negligible.

Two thermocouples were spot-welded to the bottom and the top of the oven as shown in Figure 3.61 to monitor the temperature. The thermocouple wires were Chromel (Ni/Cr), and Alumel (Ni/Al+Mn+Si).

The potassium sample used consisted of commercial potassium lumps, (99% pure). The bottom of the oven was operated at 220°C, which corresponds to 10^{-2} Torr saturated vapour pressure. This was thought to be the optimum pressure and was used in the work of Ottley & Ross (1975). 5g. of potassium lasted approximately 7 hours at this temperature, which was long enough to enable several spectra to be recorded. Many noise spikes were recorded in the spectra; these were attributed to the influence of dirt (K_2O, KOH,$\cdots$) in the sample. This was finally cured by increasing the top oven temperature to 360°C.

To produce a collimated beam at the exit of the oven, an aperture was placed there (see Figure 3.61). This aperture was a stainless steel collimated hole structure, manufactured by Brunswick-Corporation, consisting

Oven

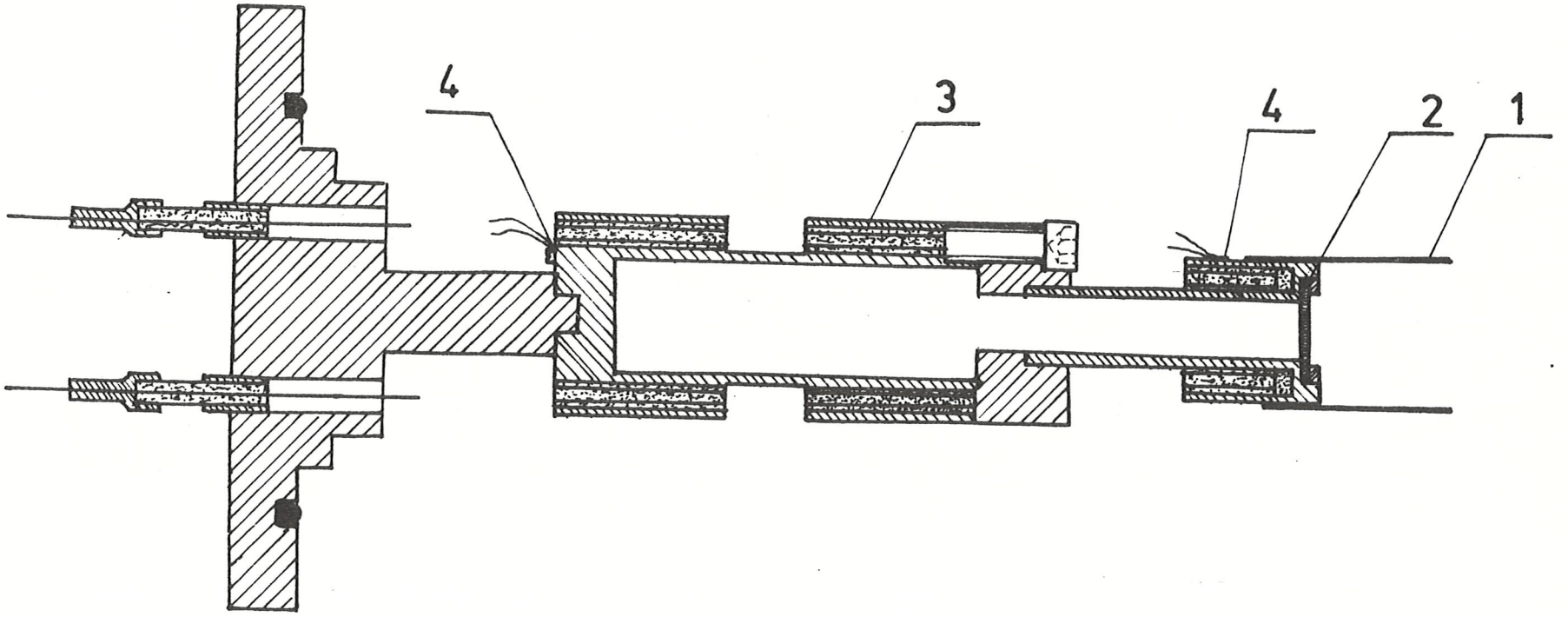

1- Copper shield

2- Collimated hole structure

3- Twin-bore ceramic tube

4- Thermocouple junction

of 5,500 holes each of 0.12mm diameter and 1.25mm length. The theory of using this type of aperture has been given by Giordmain & Wang (1960).

Maintaining the temperature at the top of the oven higher than the bulk is important in order to prevent condensation and consequent blocking of the oven aperture. It also prevents molecular recombination in the beam.

3.7 Helmholtz Coils: (Magnetic Field Neutralization)

In an arrangement due to Helmholtz, a region of uniform magnetic field is obtained midway between two equal coaxial circular coils set parallel to one another with the separation between their centres equal to the radius of the coils. In the present experiment square coils of side, 170cm were used to facilitate access to the apparatus. Two pairs of coils were used to neutralise the two earth's field components; the apparatus was alligned N-S.

With 1.4A in horizontal coils and 0.5A in the vertical coils the net magnetic field was zero. However, the optimum currents required to obtain good resolution were 0.5 in the horizontal coils and 1.12A in the vertical coils with 0.08A in the coil mounted round the analyzer (see Figure 3.321). This indicates that there was considerable residual magnetisation in the system. The magnetic field was measured using a Newport Instruments flux meter.

3.8 Liquid Nitrogen Trap (Trap and Collision Region)

The construction of the liquid nitrogen trap is shown in Figure 3.12. The bottom of the trap, a copper block welded to the stainless steel dewar, formed the interaction region. Holes were machined in the copper for the electron beam to pass through to the Faraday cup, and for the vapour beam to pass in. The vapour beam was condensed out after

crossing the interaction region.

The surface of the interaction chamber was coated with benzene soot (smoke from natural gas bubbled through benzene, contained in a flask, and burnt at the end of a tube) to reduce electron reflections and the formation of the secondary electrons.

3.9 Detection System

A schematic diagram of the detector electronics is given in Figure 3.91. The ejected electrons transmitted by the electrostatic energy analyzer were allowed to strike the inner surface of an electron multiplier (Mullard B419BL). The gain of the electron multiplier is about 10^7. The front of the electron multiplier was connected to Earth, the same potential as the Earthed slit 2, and the other end to a 5kV variable supply. The charge pulse from the multiplier is converted into a voltage pulse by the total input circuit capacitance to earth. In practice this pulse is of the order of 1mV, and the circuit capacitance $C \simeq 10^{-9}$F. It is essential to keep the input capacitance as low as possible by keeping the connecting wires between the multiplier and the emitter follower as short as possible, in order to obtain a high amplitude voltage pulse. The role of the emitter follower is to match the electron multiplier impedance ($\sim 2M\Omega$) to the input impedance of the amplifier ($\sim 50\Omega$) without changing the amplitude of the signal pulses. The output of the emitter follower was connected to an amplifier and discriminator. The output of the discriminator was connected to the input of the ratemeter, and the analogue output of the ratemeter was displayed on an XY recorder to record the spectra. A loudspeaker circuit was connected to the output of the discriminator to produce an audio signal.

Care was necessary to ensure that the multiplier was working in its plateau region. It was also important to ensure that the discriminator

Schematic diagram of detection system

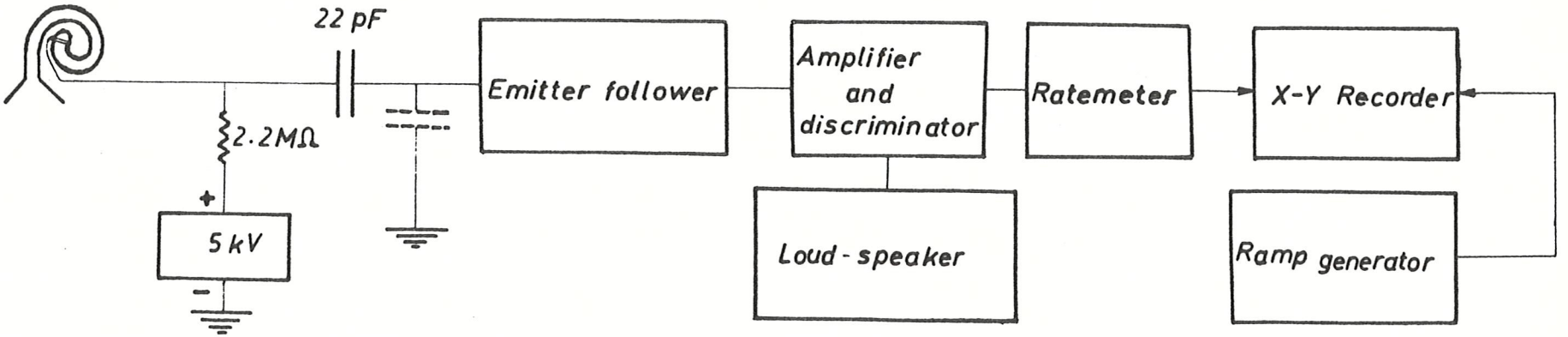

level was not set too high, since the channel multiplier gain decreases with increasing count rate, and this could lead to a loss of recorded signal.

3.10 Setting up the Spectrometer

The spectrometer was operated when the pressure was in the 10^{-6}Torr range. The electron gun was set up to provide a beam of 400, 60, or 30 eV electron kinetic energy and the current in the Faraday cup measured. The liquid nitrogen trap was filled and the oven temperature was increased in 30 minutes to the operating temperatures of 360° and 220°C for the top and base, respectively. The high voltage power supply was set at the plateau region for the multiplier, typically 3.6kV. The analyzer was set up to transmit electrons of 10eV (4V across analyzer). Neglecting the incident angular spread, this analysis energy corresponds to a theoretical FWHM of 25 meV. In practice the FWHM at this energy was approximately 55 meV. This difference clearly represents a contribution from the angular term in the expression for the resolution (see page 25).

The ramp voltage was then adjusted to a known strong feature in the spectrum ($3p^5 4s^2\ ^2P_{3/2}$ in potassium), and the detected signal was maximised by adjusting the currents in the Helmholtz coils and the coil round the analyzer, and high voltage power supply. The ramp voltage generator was used to scan the voltage between earth and the entrance to the analyzer. The entrance slit was connected to the exit slit, and they were both kept at the same potential as the centre line of the hemispheres. The analogue output of the ratemeter was taken to the Y input of the XY recorder and the ramp generator output to the X input. Spectra were recorded when the oven temperatures, and hence the potassium vapour pressure, were stable.

The system was protected with an interlock circuit which caused the

diffusion pumps and the electronics to be turned off in the event of a water or vacuum failure.

3.11 Apparatus 2

In the previous spectrometer the best resolution obtained was 55 meV. This relatively poor resolution was the result of having the front plate of the analyzer earthed. This caused field penetration into the gap between the hemispheres; and thus the electrons were defocussed to some extent; in addition there were serious difficulties with stray magnetic fields, and the analysis of the ejected electrons at 90° with respect to the incident beam gives poor resolution, because the ejected electron intensity is usually a minimum at that angle, (see page 38). The second apparatus differs in having the front plate at the centre potential of the analyzer, which greatly reduces the field penetration from the front plate. Also the analyzer was made of aluminum and is therefore non-magnetic. The best resolution obtained with this instrument is approximately 20 meV.

Apparatus 2 has been described by Ross et al (1976). The spectrometer is able to detect electrons ejected at angles up to 120° with respect to the incident electron beam. Otherwise its operation is identical to that of Apparatus 1.

The electron beam was collected in a Faraday cup, whose entrance aperture (collector) diameter was 1.5mm and was situated 130mm from the final stage of the electron gun. At high energy the beam current was focussed into the Faraday cup, while at low energy the beam current into the Faraday cup was considerably reduced due to defocussing of the beam. Four different impact energies were used in the present work: 30, 40, 60 and 400 eV. The incident beam electron current at 60 and 400 eV was 20μA, focussed into the Faraday cup, and below 60 eV this current reduced

to 2μA.

The oven to produce the atomic beam was the same in principle as the former oven (see page 28). There were, however, some differences in construction. It had a removeable central tube machined from titanium which contained the metal being studied. This removeable tube was easy to take out for cleaning and loading, without removing the oven. The oven was positioned vertically below the interaction region. The vapour beam and the electron beam intersected at 90°.

The oven was loaded with 5g.(break-seal) ampoules of 99.9% pure potassium. These were broken under petroleum spirit and loaded into the oven tube with a layer of the petroleum spirit on top of the potassium.

The oven was operated with upper and lower temperatures of 260°C and 220°C respectively. Care had to be taken not to operate at too high a temperature. The spectra were observed to deteriorate at temperatures corresponding to high vapour pressures (see Chapter 4).

The ejected electrons were analyzed using a 150° spherical sector electrostatic velocity analyzer with mean orbit radius of 100mm. Spectra were obtained by scanning the potential applied between two grids mounted in front of the entrance slit of the analyzer and the front plate of the analyzer using a voltage ramp generator. The spectra were recorded by keeping the analysis energy fixed (at 2.5 eV). Electrons passing through the analyzer were detected with a channel electron multiplier (Mullard 419BL). Pulses from the multiplier were fed into a conventional amplifier-ratemeter counting system, similar to that described in Section 3.9. The ratemeter output was displayed as a function of the voltage applied to the grids at the analyzer on a XY recorder, as described for Apparatus 1.

The spectrometer was mounted in a stainless steel vacuum chamber. The magnetic field was reduced by lining the chamber with 1.5mm thick

mu-metal. The Earth's field was reduced externally by means of Helmholtz coils. Despite this, it was found that the performance of the spectrometer depended critically on the currents in the Helmholtz coils which surrounded the apparatus.

CHAPTER 4

RESULTS & DISCUSSION

4.1 Results from Low Resolution Experiment (Apparatus 1)

In this experiment spectra were recorded at a fixed angle of 90^{o} with respect to the incident electron beam using 30, 60 and 400 eV incident electron energies. The spectrum between 13.6 and 21.1 eV ejected-electron energy is illustrated in Figure 4.11. In Figure 4.12 the spectra taken at different incident energies are compared. The numbering of the lines refer to data presented in Table 4.1. The excited-state energy scale was normalized to the ultraviolet absorption spectrum, (Mansfield 1975a), using the transitions at excited-state energies 18,722 and 22.422 eV. It was otherwise impossible to establish an absolute energy scale, due to unknown contact potential differences existing in the analyser. The ejected-electron energy scale was established by subtracting 4.341 eV (first ionization potential of potassium, (Moore, 1949)) from the excited-state energy scale. This assumes that all states autoionize into the $3p^{6}$ continuum (see page 38). The instrumental resolution was estimated by measuring the FWHM of the narrowest lines of the spectra; this is approximately 55 meV and sets an upper limit to the resolution. The spectra lie on a background of approximately 80 counts per second; this background arises principally from direct (non-resonant) ionization. In Figure 4.12 the count rate for line 1 ($3p^{5}4s^{2}\ ^{2}P_{3/2}$) above this background is approximately 2,000 and 700 counts per second at 400 and 30 eV incident energy respectively. Table 4.1 is a list of all peaks observed consistently in the spectra. The energies given are the average positions taken from four spectra. The lines have a possible error of ± 12 meV (standard deviation).

4.2 Results from High Resolution Experiment. (Apparatus 2)

Using Apparatus 2 ejected electron spectra of potassium vapour

were obtained at 50° and 75° with respect to an incident electron beam of energy 30, 40, 60 and 400 eV. The 3 to 15 eV ejected-electron energy region of the spectrum is shown in Figure 4.21, and the 14.2 to 20.3 eV region is shown in Figures 4.22 and 4.23. In Figure 4.24 the spectra taken at different incident energies are compared. Three peaks a, b and c as shown in Figure 4.21 were observed using a 400 eV incident electron beam and are attributed to Coster-Kronig transitions; these peaks were not recorded by Apparatus 1. Some energy-loss structures were observed in the 400 eV spectrum (Figure 4.23) resulting from too high an atomic beam density (see page 39). The energy scales were normalized to the ultraviolet absorption data of Mansfield (1975a), using lines at 18.722, 22.422 and 22.386 eV excited states energies as reference points. Three points were necessary due to a slight instrumental non-linearity. The ejected-electron energy scale was again established by subtracting 4.341 eV (first ionization potential of potassium, (Moore, 1949)) from excited-state energies. The instrumental resolution was approximately 20 meV. The background noise level is 100 counts per second, and the intensity of line number 1 is 1,000 and 2,000 counts per second, on Figures 4.22 and 4.23 respectively. Line 38 on Figure 4.23, which is cut off in the figure has a relative intensity of 2.58 with respect to line 43.

Table 4.2 is a list of peaks in the ejected-electron spectrum which were consistently observed using Apparatus 2. The energies given are the average positions taken from seven spectra. The next four columns indicate the incident-electron energies at which the lines were detectable. Comparisons are made with the earlier data from Apparatus 1 and those of Ottley & Ross (1975). Lines a, b and c, because of their breadth, have an estimated uncertainty in energy of 0.03 eV; all the other lines listed have a possible error of ±8 meV (standard deviation).

Table 4.3 compares the data obtained using Apparatus 1 and Apparatus 2 with those of Mansfield (1975a). Assignments for the lines, based on the work of Mansfield (1975a) and Martin et al (1969) are also given where possible.

Spectra observed at different angles to the incident beam showed little variation. The study of the angular distribution of autoionizing transitions in cadmium vapour, (Pejčev et al 1977) and sodium vapour, (Breuckmann et al, 1976 and Ross et al, 1976) reveals that there is an anisotropic ejected-electron intensity. These authors have shown that the ejected electron intensity generally has a minimum at 90° with respect to the incident electron beam.

4.3 Discussion

In comparing the present spectra with the photo-absorption spectrum of Mansfield, (1975a), it was assumed that the transitions, corresponding to the electrons from 3p inner shell, observed in the 14.2 to 20.3 eV ejected-electron energy range autoionize into the first continuum of K^+. This assumption is valid because the first excited-state energy of K^+ ((Core) $3p^5 4s$) is 24.489 eV above the ground state of the neutral atom. Therefore if any of the observed lines 1-84 in the ejected-electron spectrum correspond to autoionization into this continuum, the excitation threshold would be greater than $24.489 + 14.381 = 38.870$ eV, (14.381 being the ejected-electron energy of line 1). However, all lines 1-84, with the exception of 9 lines, were observed at 30 eV incident electron energy, (see Tables 4.1 and 4.2) and, so, most of observed lines cannot be related to transitions autoionizing into the (core)$3p^5 4s$ continuum. For the remaining 9 lines, with the exception of line 50, there is excellent agreement (to within 10 meV) with the data of Mansfield (1975a), assuming that autoionization does occur into the $3p^6$ continuum. Line 50 is

unresolved at low incident energy, probably due to the close proximity of lines 49 and 51. Thus autoionization into higher continua is energetically impossible, and lines 1-84 must therefore all result from excited states autoionizing to the ground state of the ion.

A few transitions on the 400 eV high resolution spectrum in Figure 4.23, just below 17 eV ejected-electron energy, are attributed to excitation of $3p^6 4p(^2P)$ at 1.61 eV above the ground state of neutral potassium (Moore, 1949). Such features have been omitted from the tables. It was found that these energy-loss features were only prominent when the excited-states were fairly intense and the atomic beam density was very high. An energy-loss of 1.61 eV from line 38 coincides almost exactly with line 16. However, line 16 is relatively intense at low incident energy, and may be attributable to excitation of a quartet state (see below). At 400 eV incident energy, such a line should be weak, and thus the peak which is labelled 16 on the 400 eV spectrum in Figure 4.23 is mostly due to energy-loss.

In Table 4.3 comparisons are made between the present data (excited state energies) with those of Mansfield (1975a), and Martin et al (1969), with assignments also taken from those works. The comparisons are made with Martin et al (1969) by matching the term separations, with less emphasis being placed on the actual baricentre of a term. Towards the high energy end of the spectrum it was impossible to resolve as many lines as Mansfield (1975a), and therefore it has sometimes been necessary to group together some of the absorption lines in order to make comparison with peaks in the ejected-electron spectrum. Assignments such as $(5_2)6d$ refer to a $3p^5(3dx4s)$ series limit followed by the running electron configuration. $(Core)3p^5(3dx4s)$ configuration refers to a mixture of the $(Core)3p^5 3d$ and $(Core)3p^5 4s$ configurations. The energies of these series limits, which are taken from Mansfield (1975a), are listed separately in Table 4.4.

Some of the ejected-electron lines which are strongest on spectra taken at low incident-electron energy, and are apparently absent on the 400 eV spectrum, do in fact correlate with absorption lines, for example, lines 3 and 4 are strongest at 30 eV incident energy; Mansfield (1975a) does observe these but they are weak. He assigns them as quartet states, which would account for their low transition probability from the ground state in photo-absorption. In general in electron excitation, one would expect such quartet states to be preferentially excited at low incident electron energy.

At low incident electron energy, many lines were observed which do not correspond to features in ultraviolet absorption spectra. These are often very intense, and may be attributed to excitation of electric dipole forbidden transition from the ground state. In particular, Martin et al (1969) have calculated the energies of several non-optical terms of the $3p^5 4s3d$ configuration. The agreement between these theoretical predictions and our experimental data in the energy range 19.5-21.5 eV is shown in Table 4.3, in which are also presented the ultraviolet absorption lines in this region.

The $^4P_{5/2}$ state is predicted to lie 71 meV above $^4P_{3/2}$. A feature was observed at this energy (19.868 eV state energy), but it does not appear on Table 4.2 and it was not observed in the low resolution spectrum, because it coincides almost exactly with $3p^6 4p$ energy loss from line 24. This line is denoted 4a and it seems probable that part, at least, of this feature is due to excitation of $^4P_{5/2}$. Lines 8, 10, 11 and 12 on the spectra are identified as $3p^5 3d4s\,^4F_{9/2,\ 7/2,\ 5/2,\ 3/2}$. The $^4F_{9/2}$ state is metastable and was first reported by Feldman & Nivick (1967) who measured the lifetime as 90 μS. They determined the threshold for excitation to be 19.9 ± 0.3 eV. Slavik et al (1975) in a mass-spectoscopy study of metastable autoionization states found the threshold to be about 20 eV. From the present work, an excited-state

energy of 20.397 eV is deduced. The remaining three members of the ^4F term appears to have a relatively larger probability for autoionization into the $3p^6$ continuum. Lines 6 and 7 coincide with the $3p^5 3d(^3P)4s\ ^2P_{\frac{1}{2},\ \frac{3}{2}}$ levels reported by Mansfield (1975a). The calculated positions from Martin et al (1969) lie about 230 meV higher in energy and are denoted $(^1D)^2P$ due to the use of a different coupling scheme for the core states. Lines 17 and 18 are correlated with the $(^3D)^2F$ levels of Martin et al (1969) and the agreement in positions is very good, although the separation is slightly smaller than that predicted theoretically. The $^4D_{3/2,\ 1/2}$ states were observed in the ultraviolet absorption spectrum by Mansfield (1975a) and agree very nearly with lines 21, 22. From Martin et al (1969) it is deduced that the $^4D_{7/2}$ level corresponds to line 20; the $^4D_{5/2}$ state appears to be unresolved in the present study, line 21 being on the side of the very strong line 22. The $(^1D)^2D_{5/2}$, level was calculated by Martin et al (1969) to be 54 meV below $(^1D)^2D_{3/2}$, which would place it between lines 21 and 22. This indicates that this is a very crowded region of the spectrum, where higher resolution would provide more clarification. Line 36 is probably $(^3D)^2D_{5/2}$; the theoretical separation between this state and $(^3D)^2D_{3/2}$ is 36 meV; the measured separation of lines 35 and 36 is 40 meV.

At low incident electron energies it would be expected that parity-forbidden transitions from the ground state could be excited. Martin et al (1969) predicted that the baricentre of the $3p^5 4s4p$ configuration should lie about 300 meV above the $3p^5 4s4d\ ^4F_{9/2}$ state. This is in the region of line 14. In an analysis of the work of Feldman & Novick (1967), Sprott & Novick (1968) concluded that there should be two metastable levels of potassium, $3p^5 4s3d\ ^4F_{9/2}$ and $3p^5 4s4p\ ^4D_{7/2}$ with a separation of not more than about 150 meV, although the excitation energies were found experimentally to be the same to within 0.5 eV. Lines 14, 15, 16, and an unresolved line in the region of line 17 are

attributable to excitation of the $3p^5 4s 4p\ ^4D_{7/2,\ 5/2,\ 3/2,\ 1/2}$ states.

The estimated position of $3p^5 4s 5p\ ^4D$ term is 22.9 eV; in this region there are several lines in the ejected electron spectrum (such as lines 47, 49, 50 and 51) which could correspond to this term. Other non-optical lines observed on the spectra may be due to excitation of other terms of the $3p^5 4s 4p$ or $3p^5 3d 4p$ configurations.

Lines a, b and c in Figure 4.21 have high threshold energies, and they are ascribed to inner-shell ionization processes. Lines a and b are attributed to $3s 3p^6 4s$ autoionizing into the continuum of $3s^2 3p^5\ ^2P_{3/2,1/2}$. The energies of the ejected electrons have been estimated by comparison with CaII terms. The difference in energy between $3s^2 3p^6$, CaIII and $3s^2 3p^6 4s$, CaII is 11.87 eV. Thus, as a first approximation, the $3s 3p^6 4s$ level of KII should lie 11.87 below $3s 3p^6$ of KIII which itself is 52.35 eV above the ground state of K. Thus the estimated position of $3s 3p^6 4s$ is 40.48 eV, and upon autoionizing to $3s^2 3p^5\ ^2P_{3/2,\ 1/2}$ (Coster-Kronig transitions) yields ejected electrons of 4.05 and 4.32 eV for the two J values of the final ion state, in reasonable agreement with the measured energies. The splitting of $3s 3p^6 4s(^3S_1 - ^1S_0)$ was found to be 268 meV, in exact agreement with the splitting of the final ion state. This suggests that one of the two $3s 3p^6 4s$ terms is excited preferentially. The line widths of features a and b were 170 meV.

Line c is also above the series limit for $3s 3p^6 nl \rightarrow 3s^2 3p^5$ transitions, and is possibly due to excitation of $3s^2 3p^4 4s^2$ autoionizing to $3s^2 3p^5$. This suggestion is based on the following estimate: $3s^2 3p^4(^3P) 4s\ ^4P_{av}$ has an energy of 62 eV (Moore, 1949), and thus $3s^2 3p^4 4s^2$ will lie approximately 11.87 eV below this (see above), at 50.13 eV. Upon autoionization to $3s^2 3p^5\ ^2P_{3/2}$, this yields an ejected electron of about 13.97 eV.

TABLE 4.1

Line@ Number	Incident beam energy eV 30	60	400	Ejected electron energy (eV) Apparatus 1 (Low resolution)
1*	+	+	+	14.381
2	+	+	+	14.647
4	+	+	+	15.454
5	+	+	w	15.675
6	+	+	w	15.836
7	+	+	–	15.892
9	+	–	–	16.111
10	+	+	–	16.145
11	+	–	–	16.209
12	+	+	+	16.254
15	+	+	+	16.449
16	+	+	+	16.488
17	+	+	–	16.534
19	+	+	+	16.609
20	+	+	+	16.994
22	+	+	+	17.074
23	+	r	r	17.109
24	+	+	–	17.134
25	+	+	+	17.154
26	+	+	+	17.225
27	+	+	–	17.279
29	w	w	+	17.371
31	+	+	–	17.516
32	+	+	–	17.588
33	r	+	+	17.695
37	r	+	r	18.041
38*	+	+	+	18.081
39	+	+	r	18.199
40	+	+	+	18.257
43	+	r	+	18.395
45	+	+	–	18.481
46	–	+	+	18.524
47	+	–	–	18.559
48	–	–	+	18.613
49	+	–	–	18.681
50	–	–	+	18.719
51	+	+	–	18.762
52	+	+	–	18.814
53	–	+	+	18.880
55	+	x	+	18.943

TABLE 4.1 (Continued)

Line@ Number	Incident beam energy eV 30	60	400	Ejected electron energy (eV) Apparatus 1 (Law resolution)
59	+	x	+	19.073
63	x	x	+	19.341
66	x	x	+	19.423
68	x	x	+	19.499
71	x	x	+	19.625
73	x	x	+	19.700
75	x	x	+	19.801
81	x	x	+	20.002
82	x	x	+	20.040

@ These figures are not consecutive due to comparison made with high resolution experiment - see Table 5.2.
* Calibration point - see text.
+ Line presented in spectrum at this energy.
- Line absent in spectrum at this energy.
x This part of spectrum was not recorded
w Weak line.
r Unresolved line.

TABLE 4.2

Line Number	Incident beam energy (eV) 30	40	60	400	Ejected electron energy (eV) Apparatus 2 High resolution	Apparatus 1 Low resolution	Ottley & Ross (1975)
a				+	4.52		
b				+	4.79		
c				+	13.91		
1*	+	+	+	+	14.381	14.381	14.38
2	+	+	+	+	14.640	14.647	14.64
3	+	+	w	–	15.423		15.43
4	+	+	+	–	15.456	15.454	
5	+	+	+	+	15.680	15.675	
6	+	+	w	–	15.805	15.836	
7	+	+	+	+	15.880	15.892	15.85
8	+	+	–	–	16.056		
9	+	w	–	–	16.117	16.111	
10	+	+	+	–	16.143	16.145	
11	+	+	+	–	16.207	16.209	16.17
12	+	+	+	+	16.268	16.254	16.27
13	+	+	–	–	16.304		
14	+	+	+	+	16.359		16.36
15	+	+	+	w	16.430	16.449	16.46
16	+	+	+	–	16.484	16.488	
17	+	w	–	–	16.536	16.534	
18	+	+	–	–	16.553		
19	+	+	+	+	16.609	16.609	
20	+	+	+	+	16.994	16.994	
21	+	+	–	–	17.041		17.06
22	+	+	+	+	17.076	17.074	
23	+	+	w	w	17.109	17.109	
24	+	+	–	–	17.133	17.134	17.13
25	+	+	+	+	17.155	17.154	
26	+	+	+	+	17.233	17.225	
27	+	–	–	–	17.272	17.279	
28	+	–	–	–	17.304		
29	+	+	+	+	17.366	17.371	
30	+	+	–	–	17.458		
31	+	+	–	–	17.515	17.516	
32	+	+	–	–	17.602	17.588	17.58
33	+	+	–	–	17.698	17.695	
34	+	–	–	–	17.921		
35	+	+	+	+	17.976		
36	+	w	–	–	18.016		
37	+	w	–	–	18.050	18.041	
38*	+	+	+	+	18.081	18.081	18.05
39	+	+	+	+	18.171	18.199	
40	+	+	+	+	18.254	18.257	
41	+	+	w	w	18.304		
42	+	+	+	+	18.331		
43	+	+	+	+	18.400	18.395	18.38
44	+	w	w	w	18.409		
45	+	+	w	w	18.483	18.481	

TABLE 4.2 (Continued)

Line Number	Incident beam energy (eV) 30	40	60	400	Ejected electron energy (eV) Apparatus 2 High resolution	Apparatus 1 Low resolution	Ottley & Ross (1975)
46	+	+	+	+	18.526	18.524	18.51
47	+	-	-	-	18.552	18.559	
48	+	+	+	+	18.617	18.613	
49	+	+	-	-	18.691	18.681	
50	-	-	+	+	18.711	18.719	
51	+	+	w	-	18.731	18.762	
52	+	+	+	+	18.810	18.814	
53	+	-	-	-	18.892	18.880	
54	+	+	-	-	18.929		
55	-	-	+	+	18.944	18.943	18.94
56	-	-	-	+	18.966		
57	+	+	-	-	19.004		
58	-	+	+	+	19.045		
59	+	w	w	w	19.081	19.073	
60	+	+	+	+	19.119		
61	+	+	+	+	19.204		
62	+	+	w	w	19.309		
63	+	r	+	+	19.335	19.341	19.29
64	+	-	-	-	19.361		
65	+	r	r	+	19.388		19.34
66	-	+	+	+	19.422	19.423	
67	+	r	r	+	19.451		19.45
68*	+	+	+	+	19.495	19.499	19.52
69	-	-	-	+	19.559		
70	+	+	+	-	19.588		
71	+	r	r	+	19.606	19.625	19.62
72	+	+	-	-	19.656		
73	-	-	+	+	19.695	19.700	19.70
74	+	+	r	+	19.725		
75	+	+	r	+	19.795	19.801	
76	+	-	-	-	19.829		
77	+	+	-	-	19.847		
78	-	-	-	+	19.872		
79	+	+	r	+	19.930		
80	+	r	r	+	19.955		
81	+	+	+	+	20.013	20.002	
82	+	-	-	-	20.054	20.040	20.04
83	-	+	r	+	20.073		
84	+	-	-	-	20.096		

* Calibration point - see text
\+ Line present in spectrum at this energy
\- Line absent in spectrum at this energy
w Weak line
r Unresolved line

TABLE 4.3

Line	Excited-state energy				Assignments+
	This work		Mansfield (1975a)	Martin et al (1969)	
	Apparatus 1	Apparatus 2			
1	18.722	18.722	18.722		$3p^5 4s^2\ ^2P_{3/2}$
2	18.988	18.981	18.980		$3p^5 4s^2\ ^2P_{1/2}$
3		19.764	19.759	19.614	$3p^5 3d4s\ ^4P_{1/2}$
4	19.795	19.797	19.798	19.654	$3p^5 3d4s\ ^4P_{3/2}$
4a		19.868		19.725	$3p^5 4s3d\ ^4P_{5/2}$ ++
6	20.177	20.146	20.136	20.372	$3p^5 3d(^3P)4s^2P_{1/2}$
7	20.233	20.221	20.210	20.450	$3p^5 3d(^3P)4s^2P_{3/2}$
8		20.397		20.174	$3p^5 4s3d\ ^4F_{9/2}$ ++
10	20.486	20.484		20.243	$3p^5 4s3d\ ^4F_{7/2}$ ++
11	20.550	20.548		20.306	$3p^5 4s3d\ ^4F_{5/2}$ ++
12	20.595	20.609		20.360	$3p^5 4s3d\ ^4F_{3/2}$ ++
14		20.700		21.259	$3p^5 4s4p\ ^4D_{7/2}$ ++
15	20.790	20.771		21.291	$3p^5 4s4p\ ^4D_{5/2}$ ++
16	20.829	20.825		21.310	$3p^5 4s4p\ ^4D_{3/2}$ ++
17	20.875	20.877		20.889	$4s3d(^3D)3p^5\ ^2F_{7/2}$ ++
18		20.894		20.916	$4s3d(^3D)3p^5\ ^2F_{5/2}$ ++
20	21.335	21.335		21.259	$3p^5 4s3d\ ^4D_{7/2}$ ++
21		21.382	21.403	21.291	$3p^5 4s3d\ ^4D_{5/2}$ ++
				21.310	$3p^5 3d4s\ ^4D_{3/2}$
22	21.415	21.417	21.425	21.326	$3p^5 3d4s\ ^4D_{1/2}$
23	21.450	21.450	21.455		$3p^5 3d(^1D)4s^2D_{3/2}$
29	21.712	21.707	21.702		
35		22.317	22.303		$3p^5 3d(^3D)4s^2D_{3/2}$
			22.307		$3p^5 4p^2\ ^4P$
37	22.382	22.391	22.386		$3p^5 3d(^1P)4s^2P_{1/2}$
38	22.422	22.422	22.422		$3p^5 4s5s\ ^4P_{3/2}$
39	22.540	22.512	22.506		$3p^5 4s5s\ ^4P_{1/2}$
40	22.598	22.595	22.584		$3p^5 4s(^3P)5s^2P_{3/2}$
41		22.645	22.646		$3p^5 4s5s\ ^4P_{1/2}$
43	22.736	22.741	22.729		$3p^5 3d(^3P)5s^2P_{1/2}$
44		22.750	22.755		$3p^5 3d(^3P)5s^2P_{3/2}$
46	22.865	22.867	22.856		$3p^5 4s(^1P)5s^2P_{3/2}$
48	22.954	22.958	22.956		$3p^5 4d4s\ ^4D_{1/2,\ 3/2}$
					$3p^5 4s(^1P)5s^2P_{1/2}$
52	23.155	23.151	23.142		$3p^5 4d(^1D)4s^2D_{3/2}$
55	23.284	23.285	23.285		$3p^5 4d(^3D)4s^2D_{3/2}$
56		23.307	23.315		$3p^5(4p^2\ ^1D)^2P$
58		23.386	23.379		$3p^5 4d(^1P)4s^2P_{3/2,\ 1/2}$
59	23.414	23.422	23.417		$3p^5(4p^2\ ^1D)^2D$

\+ Assignments taken from Mansfield (1975a) except where marked ++

++ Assignments taken from Martin et al (1969)

TABLE 4.3 (Continued)

Line	Excited-state energy (eV)				Assignments+
	This work		Mansfield (1975a)	Marvin et al (1969)	
	Apparatus 1	Apparatus 2			
60		23.460	23.459		$3p^5(3d^2\ ^3P)^2P$
61		23.545	23.544		$3p^5 4s 5d\ ^4P_{3/2}$
63	23.682	23.676	23.674		$3p^5 4s(^3P) 5d^2P_{1/2}$
65		23.729	23.726		$3p^5 4s 5d\ ^4D_{3/2}$ / $(5_2)6s$
66	23.764	23.763	23.761		$3p^5 4s 5d\ ^4F_{3/2}$
67		23.792	23.792		$(4_1)5d$
			23.795		$(4_1)5d$
68	23.840	23.836	23.836		$3p^5 4s(^3P) 5d^2P_{3/2}$
69		23.900	23.912		$(2_1)7s$
70		23.929	23.937		$(7_1)6s$
71	23.966	23.947	23.944		$3p^5 4s(^3P) 6d^2D_{3/2}$
			23.959		$3p^5 4s(^3P) 6d^2P_{1/2}$
72		23.997	24.008		$(3_0)6d$
73	24.041	24.036	24.035		$3p^5(4p^2\ ^1S)^2P$
			24.047		$3p^5 4s(^1P) 5d^2P_{1/2}$
74		24.066	24.061		$3p^5 4s(^1P) 5d^2P_{3/2}$
			24.087		$3p^5 4s(^3P) 6d^2P_{3/2}$
75	24.142	24.136	24.135		$(2_1)8s$
			24.143		$(2_1)8s$
76		24.170	24.173		$(1_2)9s$
77		24.188	24.181		$(2_1)7d$
78		24.213	24.206		$(5_2)6d$
			24.220		$(5_2)6d$
79		24.271	24.266		$(1_2)9d$
			24.280		$(2_1)8d$
80		24.296	24.290		$(2_1)8d$
			24.299		$3p^5 3d(^3D) 5s^2D_{3/2}$
81	24.343	24.354	24.341		$(7_1)7s$
			24.346		$3p^5 4s(^1P) 6d^2P_{3/2}$
82	24.381	24.395	24.383		$(5_2)7d$
			24.390		$3p^5 4s(^1P) 6d^2P_{1/2}$
83		24.414	24.414		$(6_0)7d$
84		24.437	24.439		$(4_1)8d$

\+ Assignments taken from Mansfield (1975a) except where marked ++

++ Assignments taken from Martin et al (1969)

TABLE 4.4

Limit	State energy (eV)
1_2	24.489
2_1	24.580
3_0	24.604
4_1	24.736
5_2	24.790
6_0	24.817
7_1	24.979

4.11

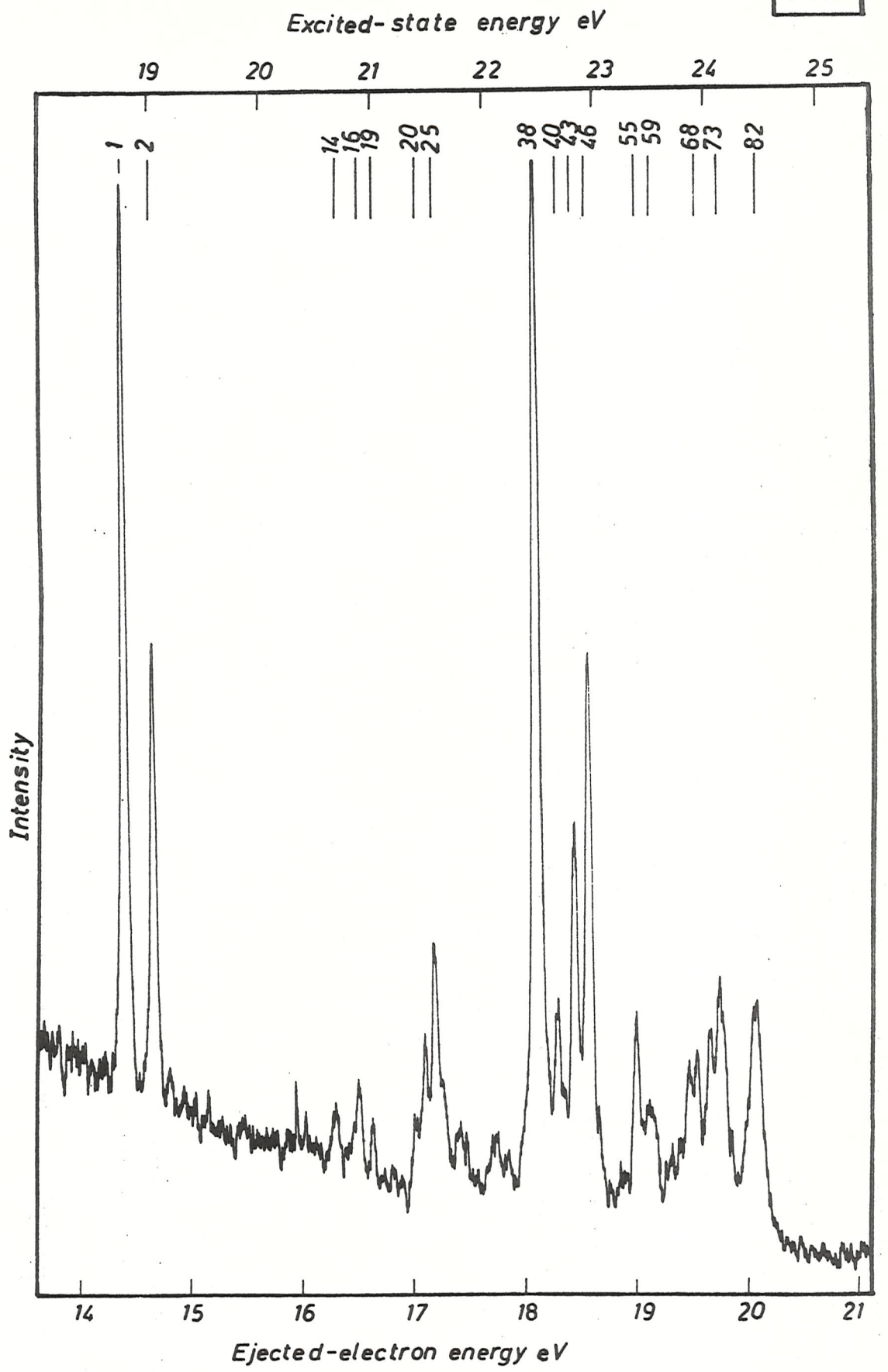
Excited-state energy eV
19
20
21
22
23
24
25
1
2
14
16
19
20
25
38
40
43
46
55
59
68
73
82
Intensity
14
15
16
17
18
19
20
21
Ejected-electron energy eV

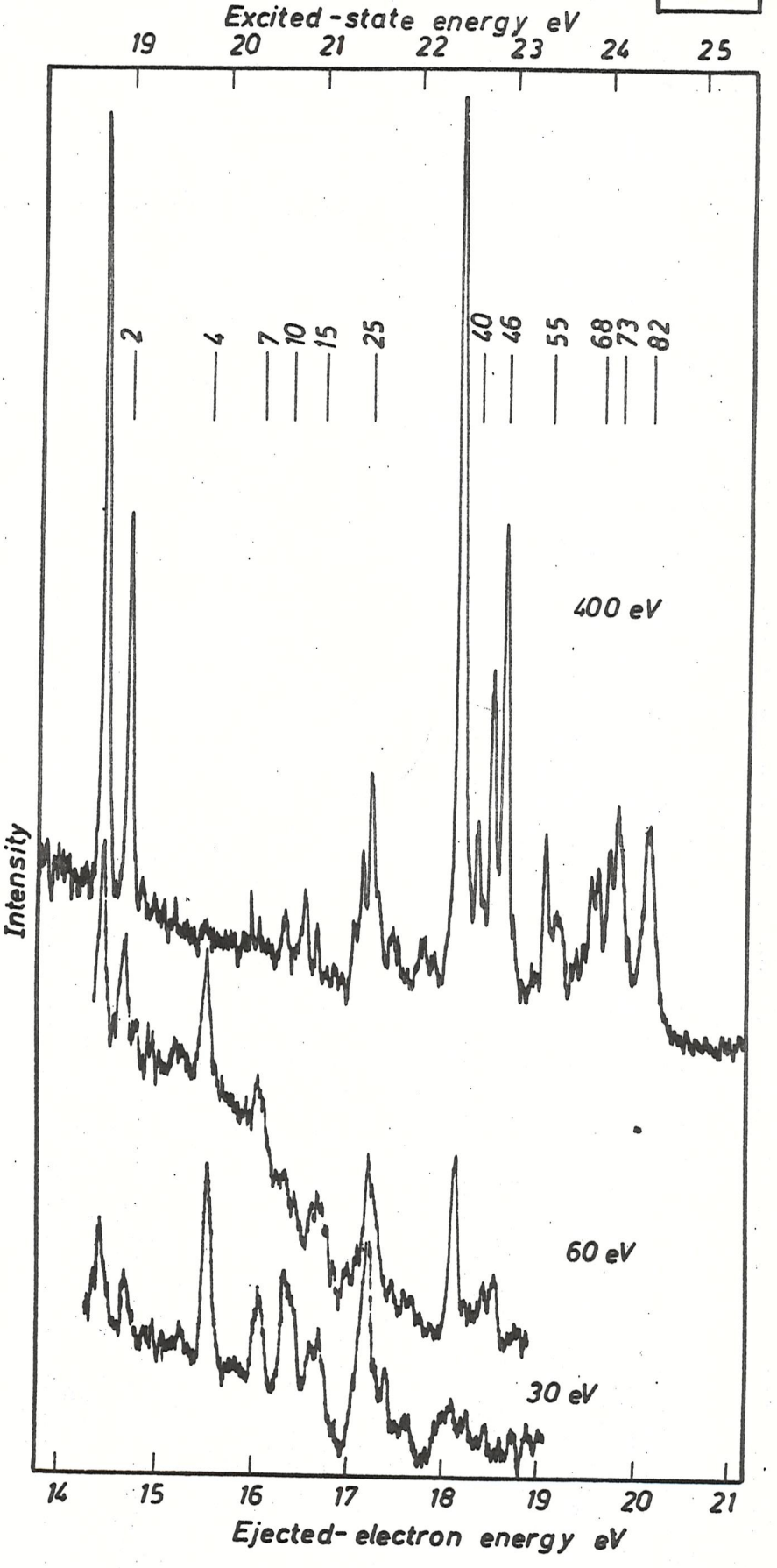
Excited-state energy eV
19
20
21
22
23
24
25
2
4
7
10
15
25
40
46
55
68
73
82
400 eV
60 eV
30 eV
Intensity
14
15
16
17
18
19
20
21
Ejected-electron energy eV

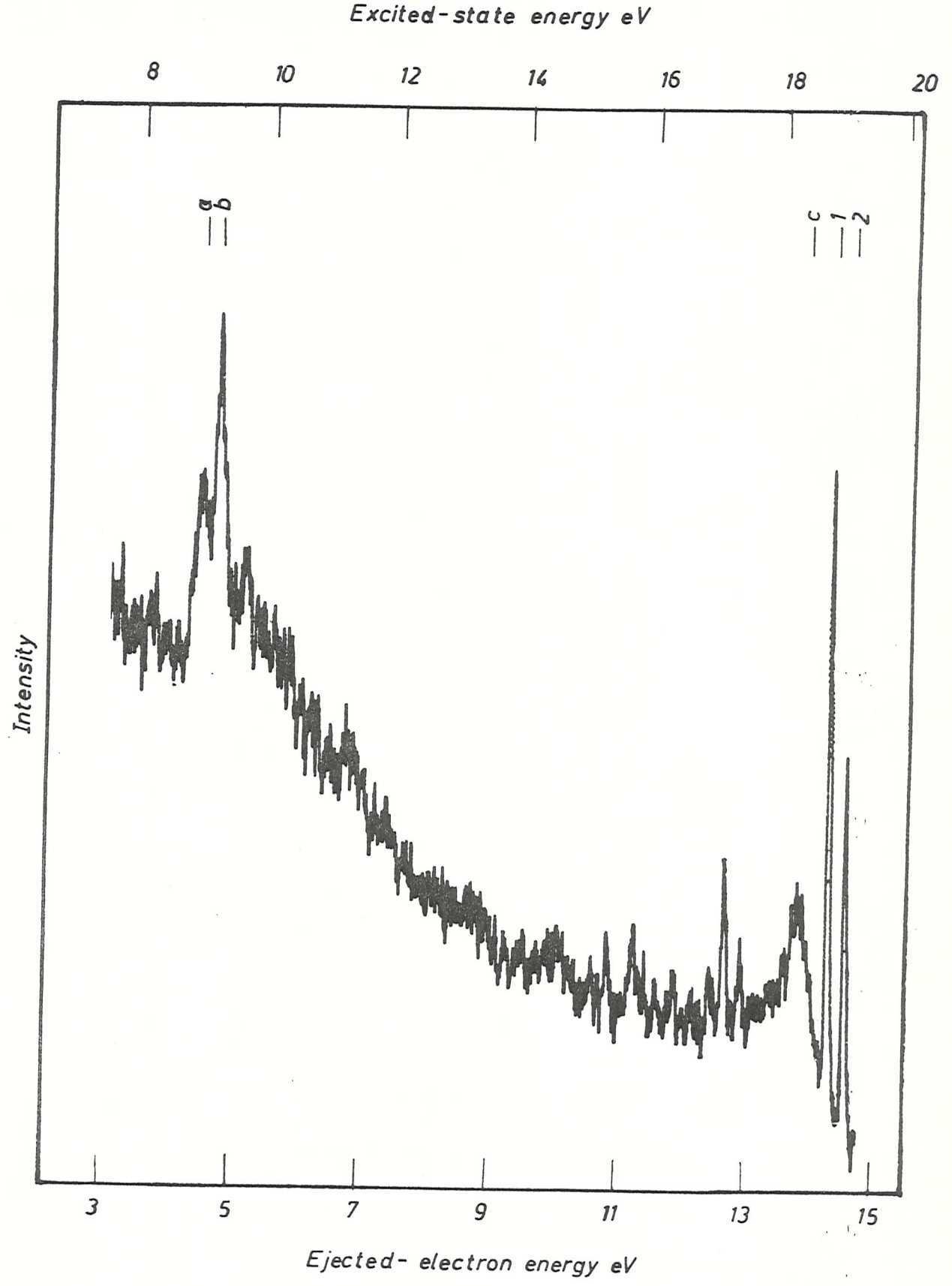
Excited-state energy eV
8
10
12
14
16
18
20
a
b
c
1
2
Intensity
3
5
7
9
11
13
15
Ejected-electron energy eV

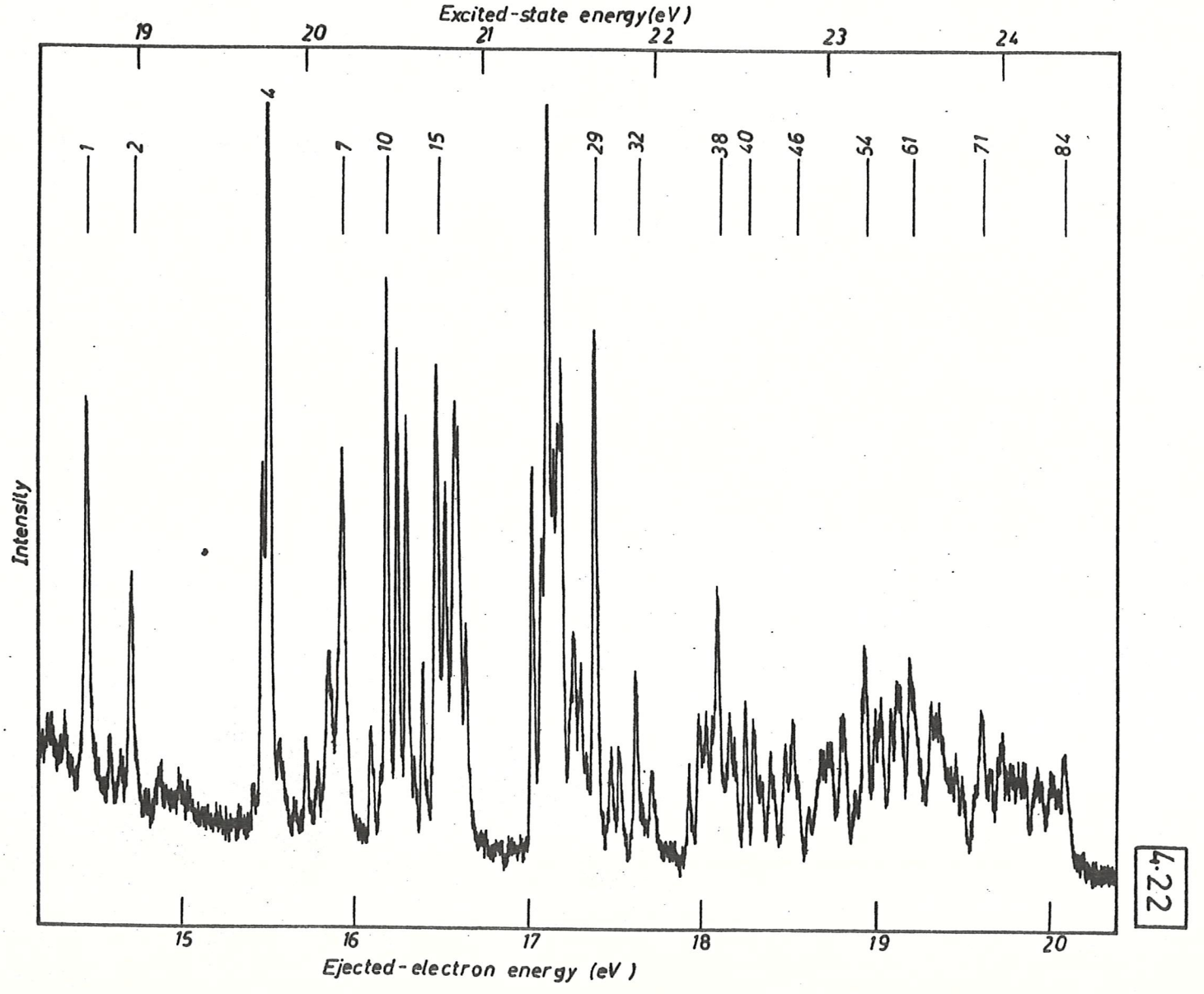
Excited-state energy(eV)
19
20
21
22
23
24
1
2
4
7
10
15
29
32
38
40
46
54
61
71
84
Intensity
15
16
17
18
19
20
Ejected-electron energy (eV)

4.22

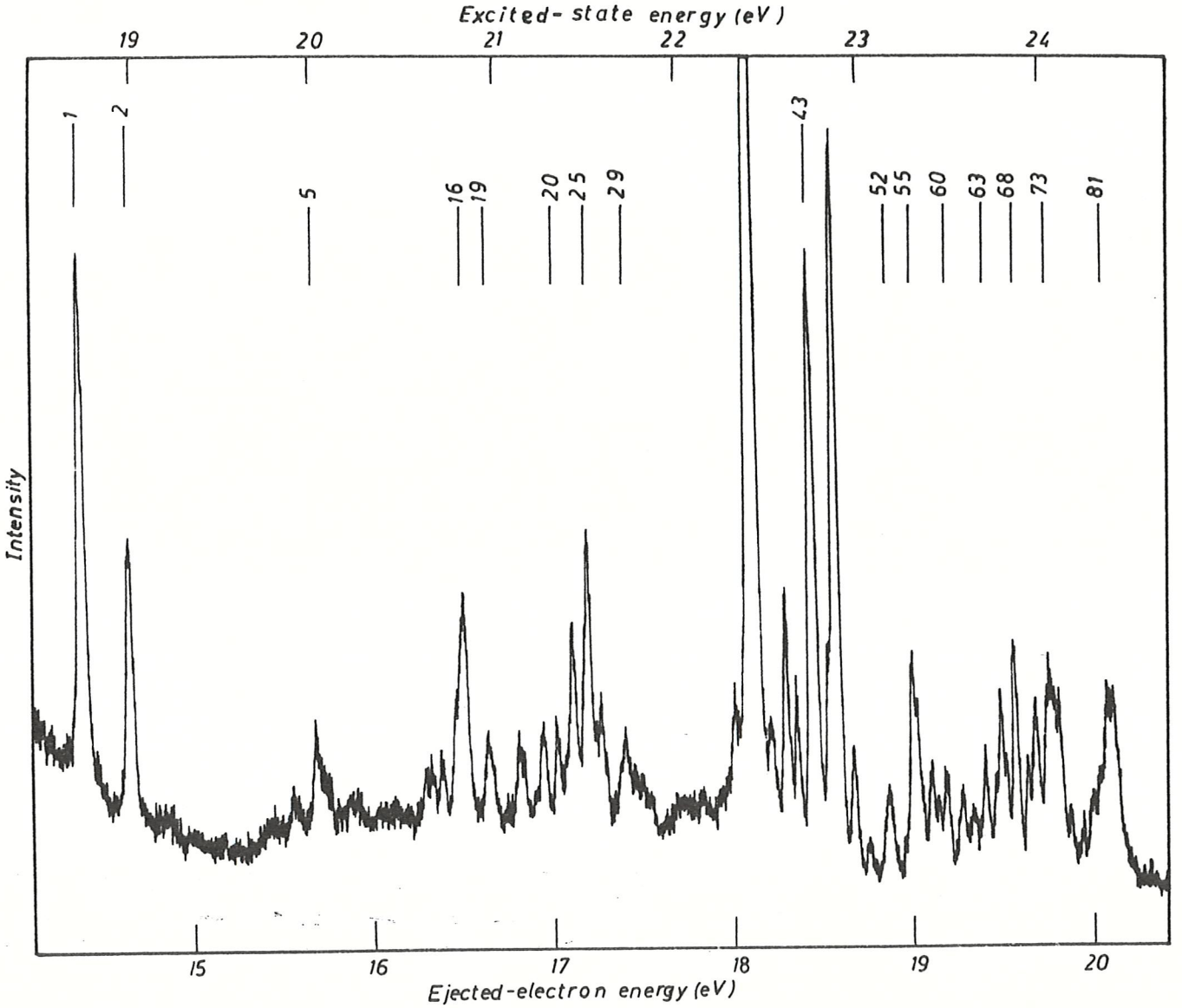
Excited-state energy (eV)
19
20
21
22
23
24
1
2
5
16
19
20
25
29
43
52
55
60
63
68
73
81
Intensity
15
16
17
18
19
20
Ejected-electron energy (eV)

4.23

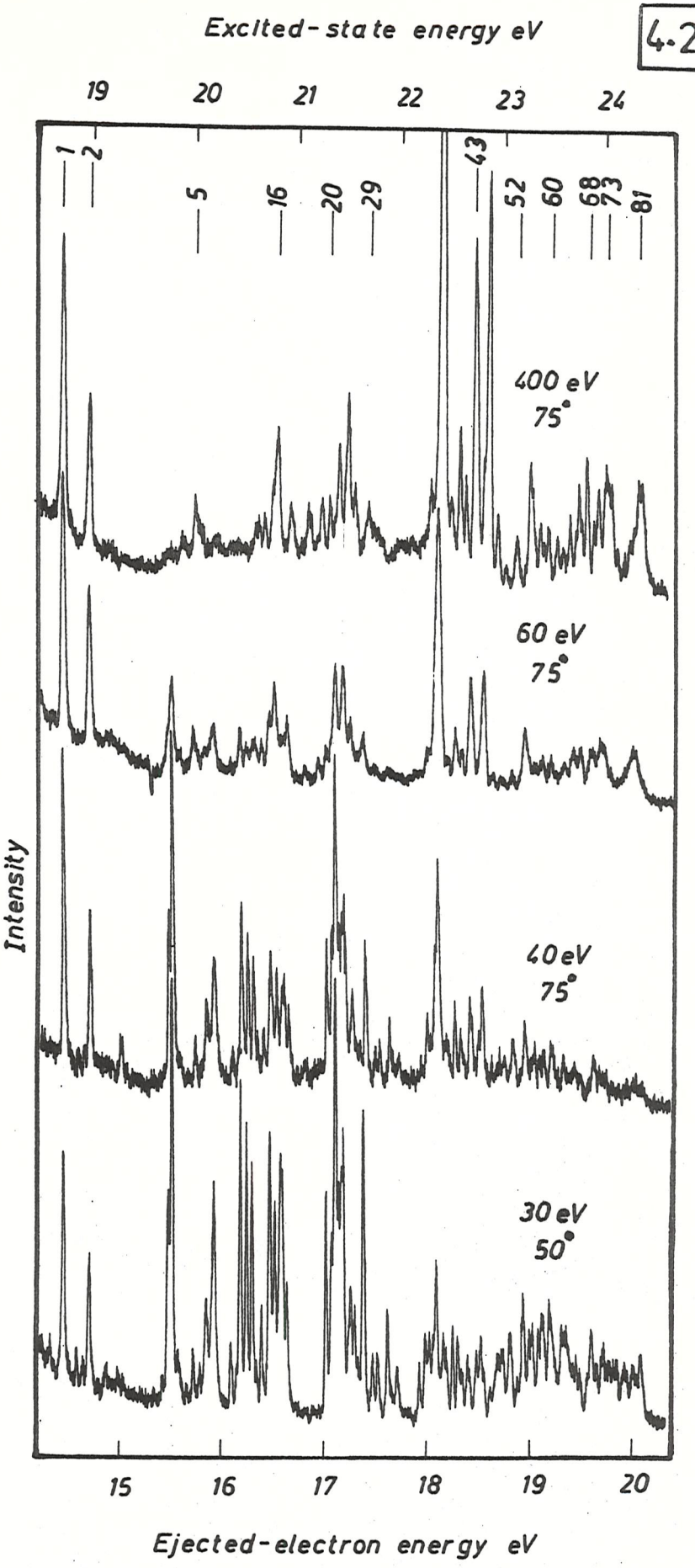
Excited-state energy eV
19
20
21
22
23
24
1
2
5
16
20
29
43
52
60
68
73
81
400 eV
75°
60 eV
75°
40 eV
75°
30 eV
50°
Intensity
15
16
17
18
19
20
Ejected-electron energy eV

Conclusion

The subject of this thesis has been the determination of energies of autoionizing levels by analyzing the electrons ejected in their decay. This, however, is only a first step and a complete investigation of these levels, using electron spectroscopy can only be carried out by observing the scattered electron in coincidence with the ejected electron. This technique is being developed in several places and results are beginning to emerge.

Autoionization has also other interesting aspects. Post-collision interaction between the ejected and scattered electrons at near-threshold excitation has been of great interest recently, and many workers have studied this effect, (Hicks et al, 1974 and Van der Wiel et al, 1976). Excitation function measurements can also be very useful to determine the type of transition involved.

Another possible direction for future work is angular distribution measurements. Some such measurements had been carried out with Apparatus 2 (Ross et al, 1976 and Pejčev et al, 1977) but an attempt to measure angular distributions of some potassium lines failed, mainly due to the change in the magnetic field and other conditions as the analyzer is rotated. This problem could be overcome by keeping the position of the analyzer fixed and varying the electron beam direction. Another reason for this failure could have been the unstable metal vapour beam which caused the line intensities to change drastically before a set of measurements could be completed. These angular distributions can potentially, be very important in studying angular momenta and other properties of the atom. However, at present the theory is not sufficiently developed to make such deductions possible.

REFERENCES

Aston F.W. 1919 Phil. Mag. 38 710

Bates, D.R. 1947 Proc. Roy. Soc. Lond. A188 350

Beutler M. & Guggenheimer K. 1933 Z.Phys. 87 188

Breuckmann E., Breuckmann B., Mehlhorn W. and Schmitz 1976 J. Phys. B: Atom. Molec. Phys. to be published.

Coster D. & Kronig R. 1935 Physica 2 13

Cowan R.D. & Andrew K.L. 1965 J. Opt. Soc. Am. 55 502

Fano U. 1961 Phys. Rev. 124 1866

Fano U. & Cooper J.W. 1965 Phys. Rev. A137 1364

Feldman P. & Novick R. 1967 Phys. Rev. 160 143

Fues E. 1927 Z. Phys. 43 762

Giordmaine J.A. & Wang T.C. 1960 J. App. Phys. 31 463

Green G.W. 1968 "The Design and Construction of Small Vacuum Systems" Chapman & Hall Ltd.

Hertel I.V. & Ross K.J. 1968 J. Phys. E 1 1245

Herzog R. 1935 Zeits. f. Physik 97 596

Hicks P.J., Cvejanović S., Comer J., Read F.H. and Sharp J.M. 1974 Vacuum 24 573

Hudson R.D. & Carter V.L. 1965 Phys. Rev. 139 1426

Hudson R.D. & Carter V.L. 1967 J. Opt. Soc. Am. 57 1471

Kuyatt C.E., Simpson J.A. and Mielczarek 1965 Phys. Rev. A138 385

Kuhn H.G. 1969 "Atomic Spectra" Longman

Mansfield M.W.D. 1975a Proc. Roy. Soc. Lond. A346 539

Mansfield M.W.D. 1975b Proc. Roy. Soc. Lond. A346 555

Martin W.C., Tech. J.L. and Wilson M. 1969 Phys. Rev. 181 66

Massey H.S.W. & Burhop E.H.S. 1969 "Electronic and Ionic Impact Phenomena" Oxford

McGuire E.J. 1972 Phys. Rev. A5 1043

Moore C.E. 1949 "Atomic Energy Levels" N.B.S., Circular No. 467 Vol. 1 (Washington, D.C.: U.S. Govt. Printing Office)

Nygaard K.J. 1975 Phys. Lett. 51A 171

Ottley T.W. & Ross K.J. 1975 J. Phys. B: Atom Molec. Phys. 8 L249

Pegg D.J., Haselton H.H., Thoe R.S., Griffin P.M., Brown M.D. and Sellin I.A. 1975 Phys. Rev. A12 1330

Pejčev V. Ross K.J., Rassi D. and Ottley T.W. 1977 J. Phys. B: Atom. Molec. Phys. 10 459

Purcell E.M. 1938 Phys. Rev. 54 818

Racah G. 1942 Phys. Rev. 61 537

Ross K.J., Ottley T.W., Pejčev V. and Rassi D. 1976 J. Phys. B: Atom Molec. Phys. 9 3237

Rudd M.E. & Smith K. 1968 Phys. Rev. 169 79

Russell H.N. & Saunders F.A. 1925 Astro. Phys. Jour. 61 38

Seaton M.J. 1951 Proc. Roy. Soc. Lond. A208 418

Shortley G.H. & Fried B. 1938 Phys. Rev. 54 739-753

Simpson J.A. & Kuyatt C.E. 1963 Rev. Sci. Inst. 34 265

Slavik V.N., Kupriyanov S.E., Perov A.A. and Kabanov S.P. 1975 Sov. Phys JETP 42 593

Soa E.A. 1959 Jenaer Jahrbuch 1 115

Sprott G. & Novick R. 1967 Phys. Rev. Lett. 21 336

Trajmar S. & Williams W. 1976 Invited lecture, VIII International Summer School and Symposium of the Physics of Ionized Gases, Dubrovnik. Text communicated privately.

Van der Wiel M.J., Wight G.R. and Tol R.R. 1976 J. Phys. B: Atom. Molec. Phys. 9 L5

Wickes J.B.P. 1975 Ph. D. thesis, University of Southampton, unpublished.